Laser Shadow Imaging of Laser-initiated Electric Prebreakdown Events in Transformer Oil

Master's Thesis by
Joachim Garmer

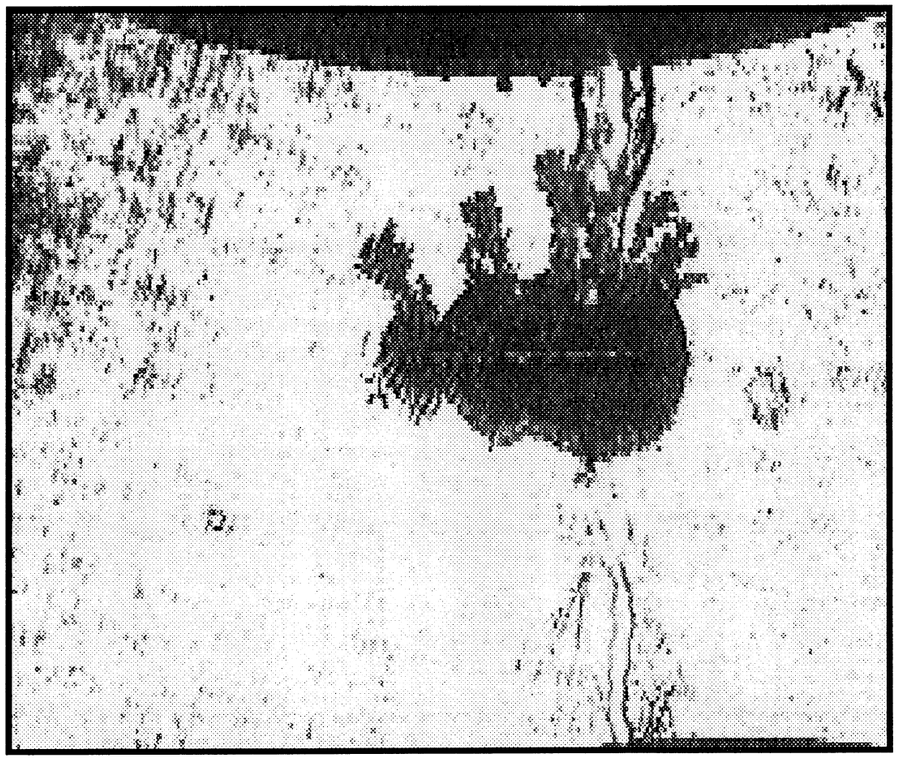

ABB

Laser Shadow Imaging of Laser-initiated Electric Prebreakdown Events in Transformer Oil

by
Joachim Garmer

Lund Reports on Atomic Physics
LRAP-199

Master's Thesis
Department of Physics, Lund Institute of Technology
ABB Corporate Research, Västerås
July, 1996

Supervisors:
Anders Sunesson
Stefan Kröll

Abstract

Focusing a laser pulse in transformer oil subjected to a strong electric field will lead to electric breakdown at a weaker electric field intensity than needed for spontaneous breakdown. Such laser-initiated breakdown processes have been imaged by the use of a second laser delivering green light. The green laser, synchronized with the initiating laser, illuminated the transformer oil prebreakdown processes with light pulses of 10 ns duration yielding extraordinary time resolution. The phenomena of prebreakdown created shadows on a CCD video camera. All the stages of prebreakdown have been imaged, including plasma initiation, vapour cavity expansion and collapse, streamer propagation, and breakdown arc. In addition, the model of laser-initiated breakdown has been slightly modified. It has been shown that cavity growth follows the Rayleigh model of cavitation and that cavity elongation due to the electric field does not take place. Propagation speed of negative streamers have been estimated to be around 200 m/s and conclusions concerning streamer connections have been drawn.

Contents

1. Introduction

1.1 Purpose and Background

The purpose of this work was to continue the studies of laser-initiated prebreakdown events in transformer oil, succeeding several different studies performed at the Department of Physics at Lund Institute of Technology. More specifically, the goal was to image these prebreakdown events and from the images gain deeper insight into the breakdown process. In other words, the main objective of this work was to record images of prebreakdown events in order to verify the existing model of laser-initiated electric breakdown (this model is descibed in Section 1.3).

The basis of this work was performed by Dag Stålhandske, who evaluated the imaging method used here [1]. This method makes use of a laser triggering system developed mainly by Anders Sunesson, ABB Corporate Research [2]. Peter Bårmann and Stefan Kröll, both at the Department of Physics at Lund Institute of Technology, and Lars Walfridsson at ABB Corporate Research also participated in the development. When a high power laser pulse is focused in a dielectric liquid subjected to a strong electric field, an electric breakdown process is initiated. In this way it is possible to control the breakdown initiation in time as well as in space. From laser triggered breakdown experiments characteristic electrode currents associated to streamer propagation (see below) have been observed [2]. This served as an incentive to this work: is it possible to image these streamers and the rest of the prebreakdown process in a reasonably simple manner?

Transformer oil is a dielectric insulating liquid used in transformers and other electrotechnical power equipment to prevent electric breakdowns and short circuits. It is also designed to support heat transport. Since the initial stages of electric breakdown in liquids are not as well known as the corresponding stages in gaseous media, it is of great importance to learn more about the liquid electric breakdown process in order to produce more reliable electric power equipment, for example transformers. One step in this direction is to record pictures of the breakdown process. So far, breakdown has been studied mainly for inhomogeneous electrode arrangements, e. g. point-plane geometries, and therefore mainly in strong and inhomogeneous field environments [2]. However, the laser triggering method makes it possible to study breakdown at weak and homogeneous fields as well.

1.2 Electric Breakdown

By definition an electric breakdown is a hot, conducting, and luminous plasma channel (arc) connecting two electrodes. A plasma is an electrically neutral, ionized state of matter. In a situation with two electrodes and an insulating dielectric liquid in between, a so-called spontaneous breakdown occurs when a sufficiently high voltage is applied to the electrode gap. The voltage level depends on gap length, electrode geometry, and properties of the dielectric liquid. Breakdown will occur at a lower voltage level if a laser pulse is focused in the electrode

gap. As mentioned above, this is the principle of laser triggering. There are other ways to trigger a breakdown, for instance by using a spark plug trigger [3, 4], but laser triggering was used throughout this work since it was important to control breakdown initiation not only in time but also in space. The electrode geometry used in this work can be seen in Figure 1.

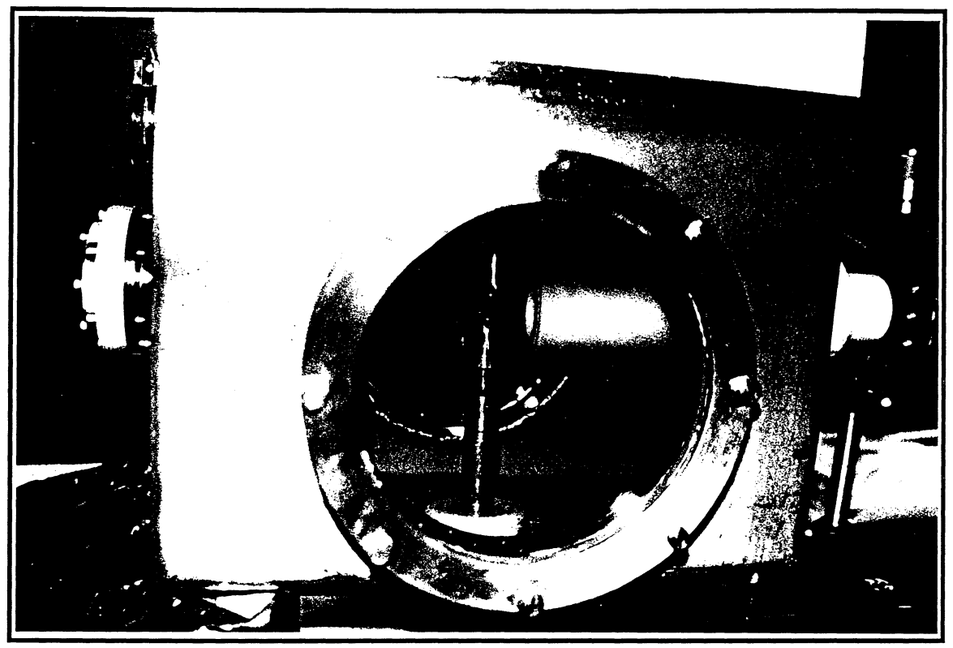

Figure 1. *Electrode arrangement used in this work. The electrodes were placed inside a so-called test cell containing the transformer oil. The white tube to the right contains a lens system.*

1.3 Streamers and Prebreakdown Processes

The actual breakdown is preceded by a prebreakdown process consisting of several characteristic events. When breakdown is laser triggered, this prebreakdown process differs from the normal one. Normally, before the real breakdown takes place, contact between the electrodes is established by so-called streamers. Streamers are filamentary plasma channels which are divided into two main groups: positive streamers grow from the anode towards the cathode and negative streamers grow in the opposite direction, i. e. from the cathode towards the anode. Thus the polarity of a streamer is known as soon as one finds the direction of propagation. Positive streamers normally grow with a propagation speed around 1-10 km/s while negative streamers usually are one order of magnitude slower [5]. Streamers can propagate in different manners and thereby be classified as either filamentary or bush-like (Figure 2). Usually, positive streamers are filamentary and negative streamers more bush-like. To conclude, the normal prebreakdown process is characterized by two main events: streamer initiation and streamer propagation.

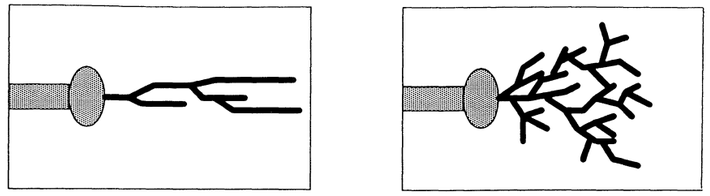

Figure 2. *Filamentary streamer (left) and bush-like streamer (right).*

The laser triggered process is different from the normal process described above, even though streamers still play an important role. A model has been derived from measurements of pre-breakdown currents and current time lags [2, 6]. A high power laser pulse which is focused into the dielectric liquid will create a plasma (Figure 3a). The heat of the plasma will vaporize the liquid and a gas bubble will be formed (Figure 3b). This gas filled cavity will expand due to high pressure (Figure 3c). A streamer will then develop out of an instability of the surface of the bubble. The streamer will propagate and connect the bubble to the nearest electrode (Figure 3d), whereupon a second streamer will bridge the remaining gap (Figure 3e). When connection between the electrodes is established, breakdown follows immediately (Figure 3f). According to this model, which seems to be the most probable of existing theories,

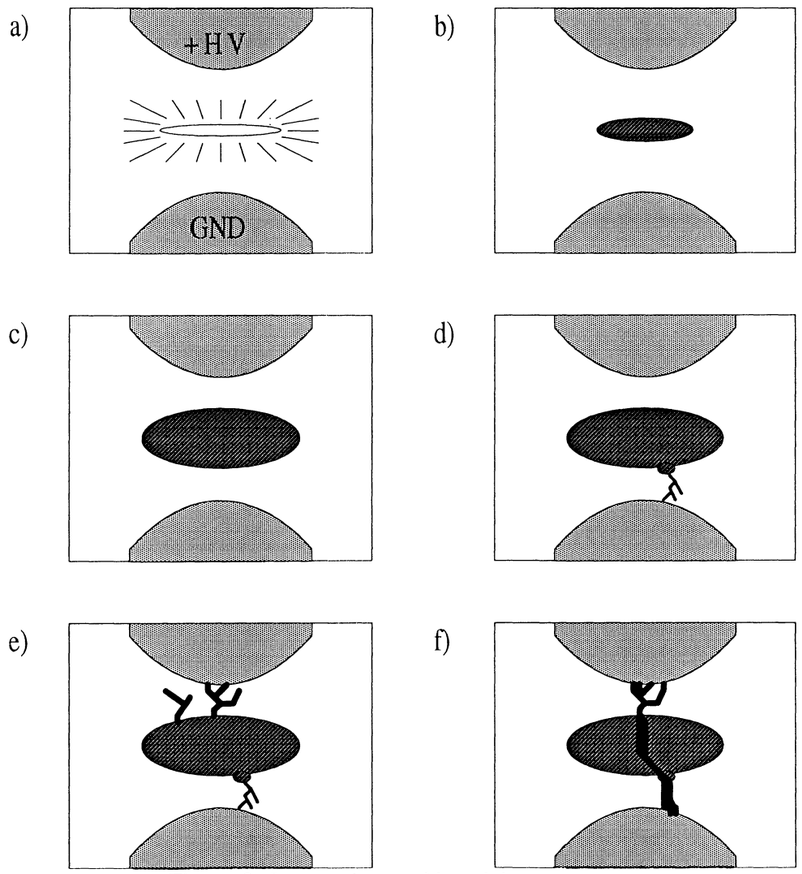

Figure 3. *Laser triggered breakdown process.*

the laser triggered prebeakdown process consists of five main events. So the objective of this work was to verify the theory of laser triggered breakdown by recording images of the different stages of the process.

1.4 The Structure of This Work

Chapter 2 deals with the equipment used and gives information on the experimental set-up. In Chapter 3, the cavity stage of breakdown (cf. Figure 3b and 3c) is discussed and the first streamer images are presented. More details about streamers are given in Chapter 4. Chapter 5 contains a summary of this work and also a look into what can be done in the future. Chapter 6 and Chapter 7 present acknowledgements and references, respectively.

2. Equipment and Synchronization

2.1 Imaging Method

The breakdown process is fast. Typically the delay time from laser trigger pulse to breakdown is some hundreds of microseconds. The intention in this work was not to take a continuous series of pictures from one single event, but rather to image the process development statistically by taking pictures from many different events in the same stage of breakdown but with only one picture for every one event. For example, to determine the size of a gas bubble at a delay time of 100 μs, ten breakdown events were initiated and ten pictures were taken, one picture per process, at this specific time. Afterwards a size average was calculated from the pictures. The method chosen here therefore did not require extreme camera picture speed, which otherwise would have been the case.

Head participants in the imaging method used in this work were a pulsed, frequency-doubled Nd:YAG laser delivering green light of 532 nm wavelength and an ordinary 50 Hz CCD video camera. The frequency-doubled laser constituted the camera light source. Since the camera was interlaced, a complete new image was formed only 25 times a second. Interlacing means that only every second line of the image is updated at a time (50 times a second in this case) in order to improve the impression of continuity. Taking single shots, this means that we get only half the picture, which is compressed vertically. In short, we lose information. Of course a non-interlaced camera is to prefer, but such a camera is also more expensive.

In spite of the slowness of the camera it was possible to take pictures having a short integration time by using the laser light source. Bubbles and streamers in the prebreakdown process can be distinguished from the transformer oil by their lower refractive index. For this reason, laser light passing through the oil is reflected and scattered from these objects and corresponding shadows are formed on the sensitive area of the camera (Figure 4). From this the term shadow imaging should be clear. The duration time of a laser pulse, 10 ns, here defined the exposure time (compare with 1 ms for an electronic shutter).

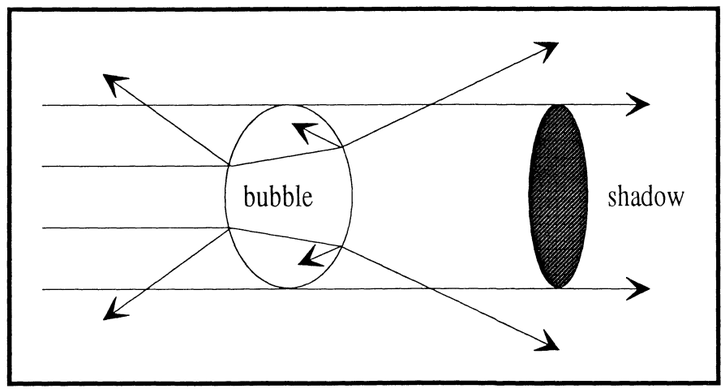

Figure 4. *Picture formation.*

2.2 EXPERIMENTAL SET-UP

Figure 5 shows the experimental configuration, which was composed of four main parts: a plasma-inducing system, an imaging system, a synchronization system and a high voltage supply system.

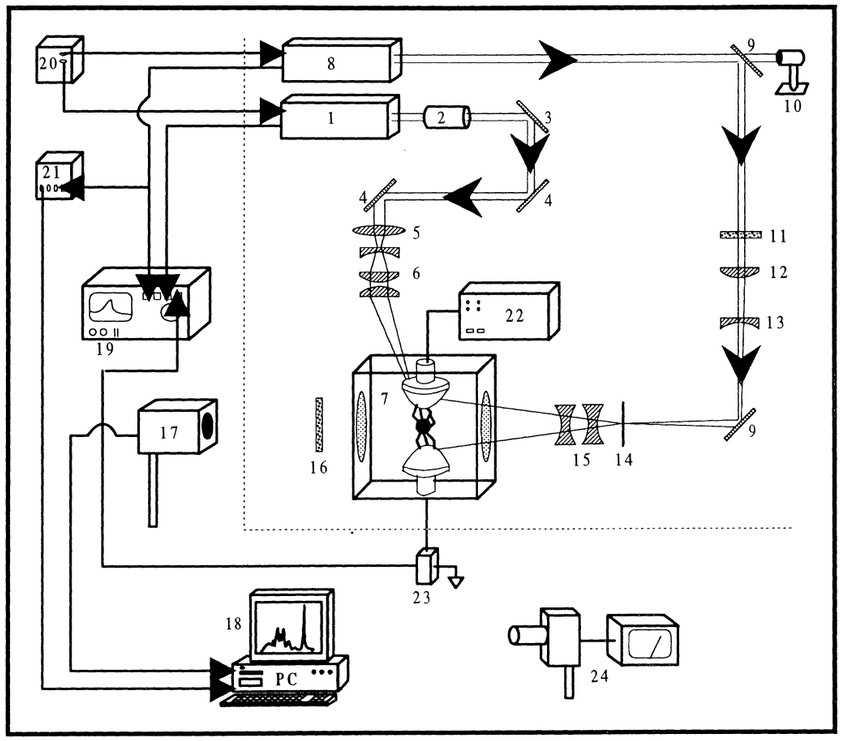

Figure 5. *Experimental set-up. Dashed line separates optics from electronics.*

Plasma-inducing system:
1) IR-laser
2) Faraday rotator
3) Prism/Mirror
4) Mirror
5) Convex lens
6) Lens system
7) Test cell

Imaging system:
8) Green laser
9) Mirror
10) Beam stop
11) Attenuation filter
12) Plane-convex lens
13) Plane-concave lens
14) Pinhole
15) Concave lenses
16) Interference filter
17) Video camera
18) IBM compatible computer

Synchronization and triggering system:
19) Digital oscilloscope
20) Pulse generator
21) Pulse conditioner

High voltage supply system:
22) High voltage supply
Miscellaneous:
23) Protection circuit 24) Power meter

In summary, focused IR-pulses from a Nd:YAG laser created plasmas at a position between two electrodes in the transformer oil. The green laser beam, perpendicular to the IR-beam, imaged the breakdown process according to the description given above. Because of its donut shaped intensity profile (cf. Figure 9 below), the green laser beam had to pass through a spatial filter before it was used to produce a shadow image of the electrode gap. A pulse generator triggered both lasers. In turn, the green laser delivered a trigger signal to a computer program called Vblsum, which captured the pictures from the video camera at the moment the green laser beam hit the electrode gap. A high voltage power source supplied a strong electric field across the electrode gap. Below is a more detailed account of each component used.

1) The plasma-inducing laser was a Quanta Ray DCR-1 Q-switched Nd:YAG laser, which delivered pulses 10 ns long at a wavelength of 1064 nm (infrared region). The maximum pulse energy available was about 350 mJ and the pulse repetition rate could be varied up to 10 Hz. Henceforth this laser will be referred to as the IR-laser.

2) The Faraday rotator, sometimes also called isolator, served to protect the IR-laser optics from backscattered light that otherwise would reenter the laser cavity. Backscattered radiation amplified in the Nd:YAG crystals could severely damage the laser, probably by destroying the Q-switch, the Nd:YAG crystals, or the output coupler. The Faraday effect or magneto-optic effect, which this device is based upon, means that the electric field direction, i. e. the polarization axis, is rotated when a static magnetic field is applied in the light propagation direction. The angle of rotation is proportional to the magnetic flux density and the length of medium traversed [7].

Used here was a Faraday rotator from Electro-Optics Technology Inc., model 1845-10. Light entering from the left is linearly polarized and then rotated clockwise by 45° as the light passes through the Faraday rotator. It then passes through a second polarizer. However, backscattered light coming from the right is also rotated clockwise by 45° when passing through the Faraday rotator and therefore ends up with a polarization which is not transmitted by the left-hand polarizer, whereby no backscattered radiation can pass.

3) In the beginning, when the number of IR mirrors was not sufficient, a prism was used to reflect the IR-laser beam at this point. Later it became possible to borrow an IR range mirror, which slightly reduced the already small energy losses.

4) These mirrors were selected to reflect IR radiation.

5) A convex lens with focal length 750 mm was needed to decrease the beam diameter so as to make the beam fit into the lens system (see below) and thereby reduce energy losses.

6) A lens system consisting of three lenses in a tube (Figure 6) focused the IR laser pulse to one spot in the electrode gap. Instead of using only one focusing lens, three lenses – the first one negative and the other two positive – were used in order to minimize self focusing effects and vary the position of the focal spot by displacing the negative lens [2]. Owing to the design of the test cell (see below) it was possible to place the lens system close to the electrodes.

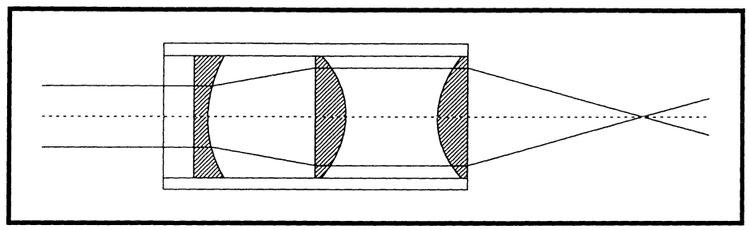

Figure 6. *Focusing lens system.*

7) The cubic test cell (Figure 7) made of stainless steel had four circular windows and contained the transformer oil and the two electrodes as well as a chain capacitor connected to the positive electrode and the grounded cell wall. In reality, the capacitor was necessary only for streamer studies. Its duty was to hold the electrode charge as long time as possible in order to keep the streamers propagating all the way to the electrodes without stopping somewhere on the way. The brass electrodes were hemispherical and had a radius of curvature of 10 mm (Figure 1). The gap length was variable. The test cell also had two smaller inlets. Through one of these was put a thin optical fibre, which was used to clean the electrode gap after breakdown. (Among other tested cleaning methods, one was to blow air into the gap through a tube, but aiming turned out to be too difficult.)

8) The camera light source was another Q-switched Nd:YAG laser from Quanta Ray, type DCR-2, yielding frequency-doubled 532 nm green pulses of 10 ns duration at a maximum pulse repetition rate of 10 Hz. The pulse energy was variable up to almost 500 mJ, but the laser was typically run at 50-100 mJ. The frequency doubler was a Quanta Ray HG-2. From now on this laser will be called the green laser.

9) These mirrors were high-power dielectric mirrors optimized for light wavelengths around 532 nm.

10) Since not all IR radiation was converted to green light in the frequency doubler, a beamstop collected the remaining IR radiation.

11) Different attenuation filters made it possible to adjust the green light intensity. Just above threshold the green laser produced pulses near the maximum allowable intensity of the camera. With an attenuation filter with 10% transmission it was possible to run the laser at a slightly higher and more stable energy level.

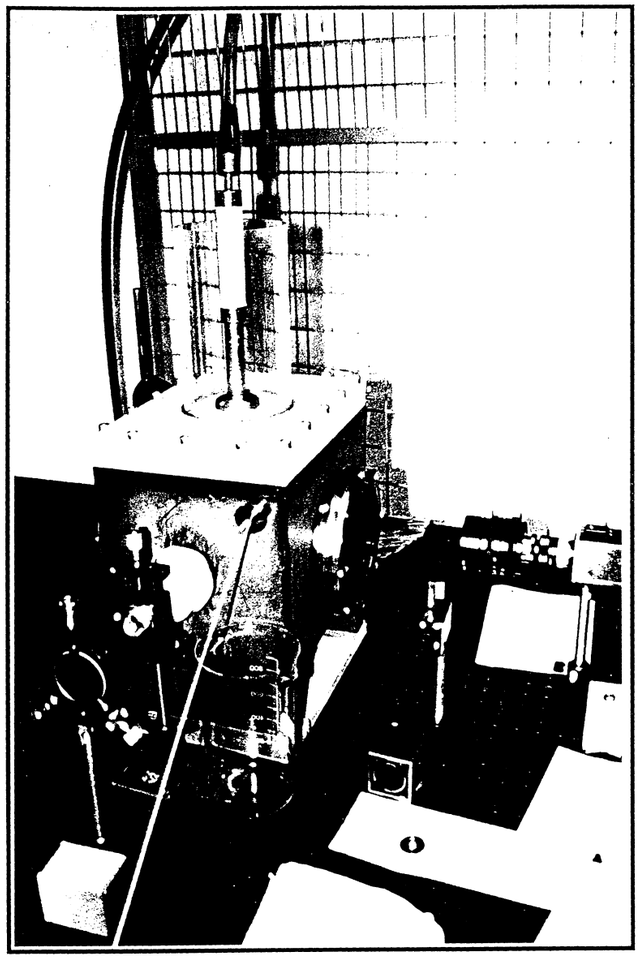

Figure 7. *Test cell and surrounding equipment. To the left is the focusing lens system, where the IR-laser light entered. The video camera can be seen to the right. On top of the test cell is the high voltage connection.*

12-14) A plane-convex lens with a focal length of +400 mm, a plane-concave lens with a focal length of –100 mm, and a pinhole with a radius of 50 µm constituted a spatial filter (Figure 8). Spatial filtering was necessary because of the donut shape of the green laser beam profile (Figure 9), which is due to the unstable resonator design of the laser. However, this kind of resonator allows a more efficient energy extraction from the oscillator rod. Spatial filtering is a process where certain spatial frequencies are partly or completely blocked out. In this case, a small circular aperture (the pinhole) removed high spatial frequencies of the laser beam. Detailed information can be found in reference [1].

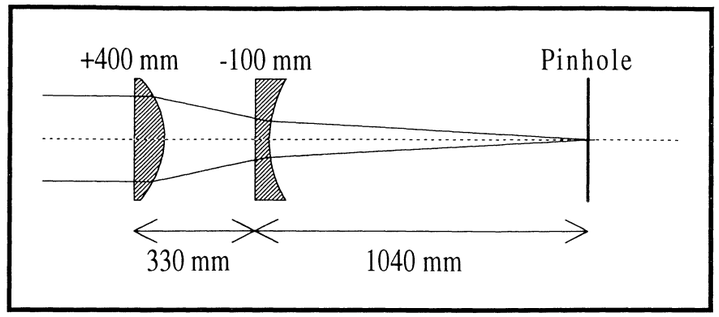

Figure 8. *Spatial filter.*

The lenses were 330 mm apart and the distance from the plane-concave lens to the pinhole was 1040 mm. The reason for a configuration with two lenses instead of using one single focusing lens was that in this way the beam path length was reduced nearly three times. The focal length became 4000 mm, but the system only occupied 1370 mm. The focal length had to be this long since a pinhole of macroscopic size was desired. A shorter focal length would have demanded a much smaller pinhole and therefore sophisticated techniques to create it*.

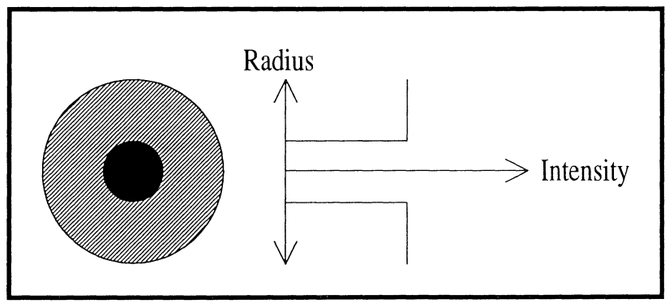

Figure 9. *Laser beam cross-section and approximate intensity distribution.*

15) Concave lenses expanded the beam diameter to make it sufficient for the object (electrode gap) and the camera.

16) An interference filter made by IR Industries Thin Film Products with maximum transmission (57%) for green light (centre wavelength 533 nm, bandwidth 5.0 nm) was used in order to suppress disturbing light from the breakdown arc and streamers in the breakdown process.

17) The image detector was an OSCAR 420D charge coupled device (CCD) 50/25 Hz interlaced video camera equipped with customized lenses which allowed of to scale true reproduction, i. e. no object magnification. The dimensions of the sensitive CCD area were 6.4

* Since the effective diameter of a focused gaussian spot is given by $d = f\lambda/a$ [8], where f is lens focal length, λ is laser wavelength and a is beam radius at $I_0\exp(-2)$ with I_0 as beam centre intensity, this is also the expression for the optimum pinhole diameter d for a beam with gaussian intensity profile. While spatial filtering actually was necessary for the green laser beam because of its non-gaussian shape, this note mainly serves as an implication to the fact that pinhole diameter is proportional to lens focal length.

mm × 4.8 mm with 542 × 492 pixels. Since preserving the correlation between light intensity and picture brightness was important, automatic gain control was turned off. For the same reason, gamma correction was set to 1. Automatic gain control provides higher gain for low light intensities than for high light intensities. Gamma correction is an opportunity to modify picture contrast according to the sensitivity of the human eye. With this constant being 1, the relation between light intensity and output signal is linear.

18) Pictures from the camera were sent to an IBM compatible computer with a 486 33 MHz processor. Installed was a Videoblaster card with accompanying Videoblaster software and also a non-commercial program called Vblsum. Vblsum, written in Turbo Pascal at the Department of Physics, was originally developed for another project, where video pictures were to be summed up. This explains the abbreviation Vblsum. Vblsum made it possible for me to automatically freeze the picture from the video camera. Expressed differently, the video camera picture was captured by Vblsum at a specific time given by an external trigger signal. This subject will be returned to in the following section.

19) For signal surveillance and delay time measurements a Tektronix TDS 540 digital oscilloscope was used. This oscilloscope offered an analogue bandwidth of 500 MHz and 1 GHz sampling rate. Breakdown currents were observed after having passed the protection circuit (23).

20) The repetition rate of the lasers and the triggering of Vblsum were governed by signals from this home-made pulse generator. Delivered signals were about 12 V in amplitude and 100 µs long.

21) Another pulse generator, a Hewlett-Packard 8003A, was used for pulse shaping purposes. Signals from the lasers were too short to be detected by the computer and Vblsum. This pulse generator increased the pulse length from a couple of microseconds to some milliseconds.

22) High voltage for the test cell electrodes was provided by a FUG HCN 35M-65000, which was capable of delivering 65 kV of either polarity. For security reasons it was fused so as in the case of a breakdown it would automatically shut down if the current would exceed a pre-set maximum level.

23) A protection circuit [2] was installed between the test cell and the digital oscilloscope in order to protect the latter from high breakdown voltages.

24) The laser pulse energy was measured with an integrating power meter, Scientech Astral AA30.

Ordinary coaxial cables were used except for the connection from the protection circuit to the oscilloscope, where a coaxial cable with an additional metallic shield was needed.

2.3 Synchronization Aspects

As may be clear from previous sections, the idea was for the IR-laser to induce an electric breakdown in the transformer oil and immediately afterwards, i. e. within a few hundreds of microseconds, the camera was supposed to detect a picture of the breakdown by means of the green laser. For this to be accomplished synchronization was required. In addition, a single shot procedure with opportunity of adjusting the delay time from IR-laser shot to green laser shot was considered eligible. An accuracy of 1 μs was desired. The green laser should fire a pulse at a certain variable time after the IR-laser shot and simultaneously Vblsum should capture a picture from the camera.

2.3.1 Laser internal timing

The fact that the two lasers were not of exactly the same type made things a bit complicated. The lasers did not have equal internal timing sequences and they offered several different ways of external triggering. According to Quanta Ray user's manuals, the lasers could be externally controlled in detail. For example, one way of running the green laser would be to trigger its oscillator and flashlamps as well as its Q-switch (Q-switching is explained below). Of course an easy triggering method was preferable instead of controlling all individual steps in the laser process like this.

First of all it was necessary to study internal timing of the lasers to determine internal time delays and signal behaviour. Information about which laser was the faster one was desired to know which laser to delay. Moreover, a signal suitable for Vblsum triggering was wanted; each laser was able to generate four synchronization output signals: oscillator, flashlamp, Q-switch, and variable (with respect to Q-switch output). Another interesting question was if laser internal timing would depend on triggering signal width, for example. After having studied the user's manuals, flashlamp triggering with internal Q-switch operation seemed to be the most appropriate method, but since it was not known which triggering signals really were the best in this case, a couple of different signal measurements were performed.

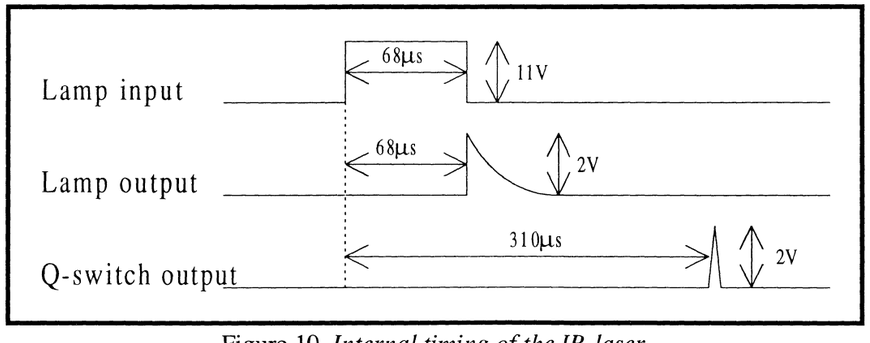

Figure 10. *Internal timing of the IR-laser.*

When the IR-laser was triggered through the lamp synchronization input control, the lamp output delay stayed at 68 μs as long as lamp input width exceeded 68 μs. With this same condition fulfilled, Q-switch output delay proved to be around 310 μs (Figure 10). These time intervals

varied a little from day to day, typically a few tens of microseconds. With two pulse generators at disposal, it was also made sure that delaying of lamp input did not have any effect on Q-switch output delay.

Concerning the green laser, lamp output delay was always equal to lamp input signal width, i. e. the lamp output signal responded to the falling edge of the lamp input signal (Figure 11). Q-switch output delay also varied with lamp input signal width. Using a width of 100 µs, this delay was approximately 330 µs. Since the Q-switch output signal looked "spiky," it was replaced by the variable synchronization output signal. Timing was set to exactly match the Q-switch output signal. As for the IR-laser, a lamp input delay influenced neither the Q-switch output delay nor the variable output delay.

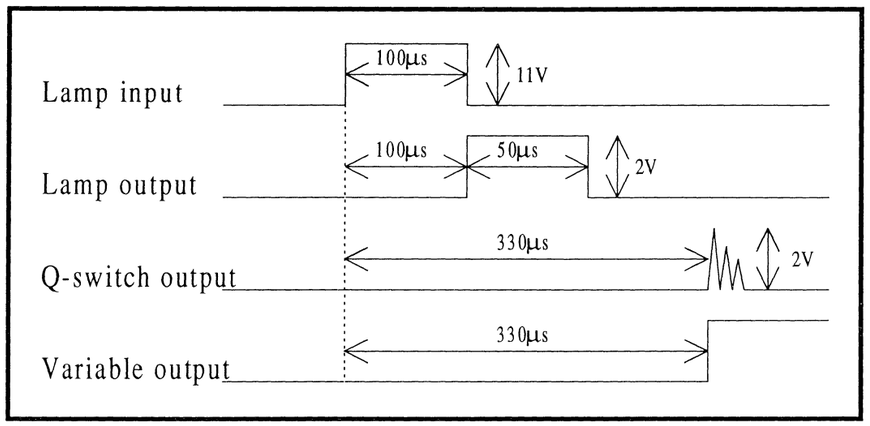

Figure 11. *Internal timing of the green laser.*

2.3.2 Q-switching and pre-triggering of high voltage relay

At this point a discovery, which seemed very important at first, was made about the green laser external control. According to the user's manual, provision had to be made to pre-trigger the high voltage relay of the laser. The purpose of this relay is to increase the lifetime of the Q-switch by reducing the time the high voltage is applied. Twenty years ago it was not possible to obtain a sufficiently fast high voltage rise time – "sufficiently fast" meaning several kV in a few tens of nanoseconds. Fast fall time was easier to accomplish. Therefore, unlike today's modern Q-switches, the laser pulse is delivered when the voltage applied to the Q-switch has dropped from a high initial value down to zero. In this way the Q-switch has to endure high voltage levels for several milliseconds (Figure 12).

Pre-triggering of the high voltage relay would demand a much more complex synchronization, for instance by activating the relay through the oscillator synchronization input control while firing the flashlamps externally at a time earlier than the internal flashlamp trigger pulse generated by the oscillator input. Thus it was a relief to find that a jumper on the relay board, controlling the Q-switch high voltage level, was already set in the CONT position (and not in the NORM position for normal operation), meaning that high voltage was applied to the Q-switch continuously. Even though this method is not at all recommended by Quanta Ray, who

claims that the lifetime of the Q-switch may be seriously impaired, a chance was taken to defeat the high voltage relay and the Q-switch was left in continuous mode. In this way the pre-triggering of the high voltage relay was avoided.

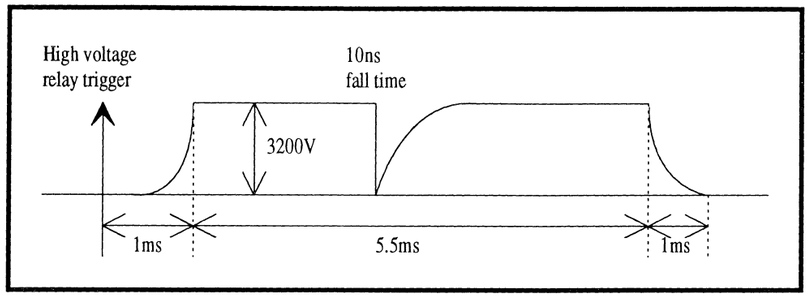

Figure 12. *Q-switch high voltage.*

To elucidate previous paragraphs, an explanation of the principles of Q-switching is in order. Q-switching is a widely used laser technique in which a laser pumping process is allowed to build up a much larger than usual population inversion inside a laser cavity, while keeping the cavity itself from oscillating by removing the cavity feedback or greatly increasing the cavity losses – in effect by blocking or removing one of the end mirrors. Then, after a large inversion has been developed, the cavity feedback is restored using some rapid modulation method. In other words the cavity Q is "switched" back to its usual large value. The result is a very short, intense burst of laser output which dumps all the accumulated population inversion in a single short laser pulse.

The green laser as well as the IR-laser used an electro-optic modulator known as a Pockels cell. Most Nd:YAG lasers do. When certain kinds of birefringent crystals are placed in an electric field, their indices of refraction are altered by the presence of the field [7]. This Pockels effect is directly proportional to the applied field strength. In the Pockels cells used here, the KD^*P (potassium dihydrogen phosphate) crystal is placed between electrodes arranged so that light passes in the same direction as the electric field. The relative transmission does not vary linearly with applied voltage, but the transmission grows as the high voltage is increased.

2.3.3 Vblsum triggering

The variable output signal of the green laser was supposed to trigger Vblsum, but this did not work satisfactory – a problem already pointed out by Stålhandske [1]. At a rough estimate only every fourth signal was successful. At first Vblsum and the computer hardware were under suspicion, but the solution was to increase the signal width by a factor of 1000, from a couple of microseconds to a couple of milliseconds. In this way every single one trigger signal was made detectable to the computer printer port. Since this was realized by means of a pulse generator (number 21 in the list above), the signal amplitude at the same time was increased from 2 V to 10 V.

2.3.4 Synchronization

Finally, synchronization was put into practice. An overview is given in Figure 13. A home-made pulse generator (number 20 above) with single shot feature and several output channels controlled the laser triggering. The signals delivered were 12 V in amplitude and 100 µs long. They could be individually delayed from a few microseconds to several milliseconds. Both lasers were externally triggered through their lamp control inputs. The Q-switch output signal of the IR-laser as well as the variable output signal of the green laser was considered to be simultaneous with the laser light pulse as the real time difference was only about 100 ns. The goal of an accuracy of less than 1 µs in the preset time difference from IR-laser shot to green laser shot was met. As also shown in the figure, Vblsum was triggered by the variable output signal of the green laser.

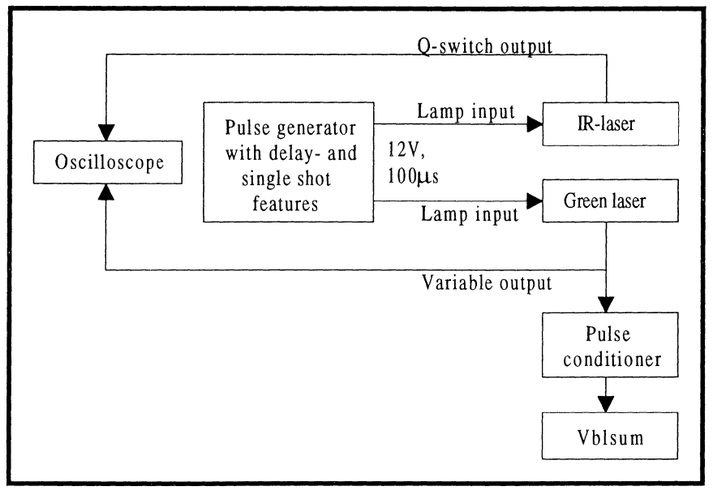

Figure 13. *Synchronization overview.*

2.4 PICTURE PROCESSING

From Vblsum, captured pictures were saved onto the harddisk of the computer. The only picture format available was a bitmap format (.BMP) with each picture element corresponding to an 8-bit value. This caused a minor problem, since the graphics processing program used for picture analysis, Micrografx Designer 3.1, did not accept bitmap files. For this reason the pictures had to be converted into an acceptable format. ZSoft Corporation PhotoFinish 1.0 was used to convert the pictures into tag image format (.TIF), but Designer was more suitable than PhotoFinish for measuring purposes. Measuring was performed without compensating for interlacing, i. e. the pictures were not expanded vertically before measuring. More about measuring procedures is given in Section 3.2.

2.4.1 Videoblaster settings

The Videoblaster software was implicitly active through Vblsum, and therefore Videoblaster Setup settings played an important role to the character of the pictures. Since the video camera delivered to scale true pictures, it was natural to set picture size according to the size of the CCD. This implied a picture size of 542 × 246 pixels (492/2 = 246 to take interlacing into account). However, Videoblaster did not work properly with this setting because the program did not incorporate the pictures completely. An innumerable number of different Videoblaster settings were tried out, but at last it was decided to treat the scale problem differently. The Videoblaster program was left with the following settings, which made it attain to given demands:

Input Interlace = OFF
Crop...
    Video Start = 6
    Start X = 0
    Start Y = 0
    Width = 881
    Height = 400
Align Video...
    Display Window X = 124
    Display Window Y = 22
    Display Position X = 16
    Display Position Y = 22
    Shift Clock Start = 0
    Interlaced Output = Disable
    Replicate Field = Disable
    800 × 600 = ON

Since this description was merely for the record, it will not be commented on any further. Refer to the Videoblaster user's manual for more detailed information. Note that the picture aspect ratio was kept: 881/400 = 542/246.

2.4.2 Scale and resolution

To determine the scale of the pictures, a ruler was photographed. The ruler pictures were processed through PhotoFinish and Designer as described above. It was concluded that 5 mm horisontally (x-direction) corresponded to a picture size of 43 mm and that 5 mm vertically (y-direction) corresponded to a picture size of 23 mm. Thus x-scale was 5/43 = 0.12 and y-scale was 5/23 = 0.22.

According to previously performed studies [1], picture resolution proved to be around 20 μm, since it was possible to resolve two lines only two pixels apart.

3. Observation of Bubble Growth from Laser-initiated Plasma

When a focused laser pulse hits a dielectric liquid like transformer oil a plasma will be formed. The plasma will exist for some hundred nanoseconds [6] and heat and vaporize the liquid whereupon a gas bubble will be created. As one of two major prebreakdown phenomena, bubble growth was the first to be examined in this work. Streamers were not yet of main interest. The intention was to visually verify the dynamics of a vapour cavity in transformer oil and to present bubble size development over time. As other similar experiments have shown [3], the bubbles have expanding and collapsing phases. To begin with bubble growth was studied without applying any high voltage to the electrodes, i. e. the bubbles were not subjected to an electric field. Later on, field studies were performed as well.

3.1 Input Pulse Energy Considerations

Bubbles were initiated at several different laser pulse energies. The pulse energies were measured outside the test cell, immediately before the laser pulses entered the focusing lens system. However, pulse energies stated in this work are corrected for reflection losses in the lens system and the test cell entrance window and also for absorption losses in the transformer oil (Figure 14). Thus, given energy values, representing pulse energies at the focal spot, are maximum available energies for plasma formation. The maximum energy transmission of the lens system was measured to be approximately 73%, which is in accordance with the theoretical limit (six lens surfaces, each with 96% transmission, give a total transmission of 0.96^6 = 78%). Entrance window transmission was 96% and energy absorption in the transformer oil was accounted for by an absorption factor of the form $1-\exp(-\alpha \cdot x)$. With the absorption coefficient α equal to 4.9 m^{-1} [2] and the in-oil-distance x equal to 17 mm, this implied an oil transmission of 92%. Consequently, the total energy correction factor was $0.73 \cdot 0.96 \cdot 0.92$ = 64%.

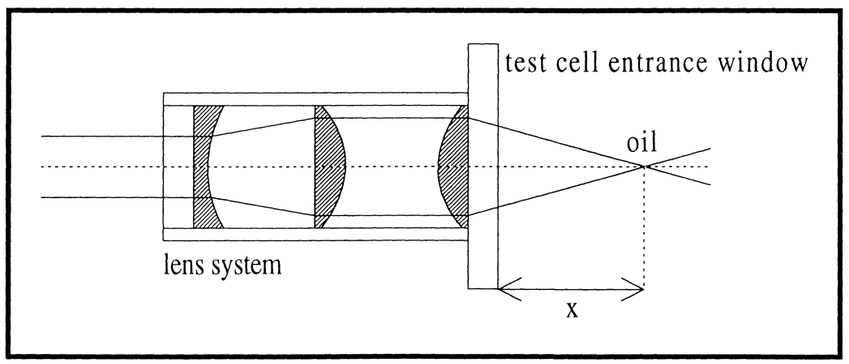

Figure 14. *The laser pulse passed through the lens system, the test cell entrance window, and a distance x in the transformer oil.*

It is important to note, however, that actual pulse energy available for plasma and bubble formation also strongly depended on the quality of the focus, which not always was as good as desired. The reason for this was practical and had to do with the design of the lens system. Because the lenses were not adjusted exactly on the optical axis it was possible to enhance the focus quality by rotating the tube containing the lens system. However, because of the off axis misalignment, rotation unfortunately also influenced the location of the focal spot. Therefore, to keep the focal spot in a certain position it was not always possible to maximize pulse energy and vice versa. In other words: transmitted energy depended on lens system turning angle. For this reason the turning angle was kept constant during the introductory, zero electric field bubble experiments, but this was not possible when it was time to go on with electric field studies, since the focal spot had to be moved to a position within the electrode gap. The zero electric field studies were perfor-med outside the electrode gap so as to avoid any influence by the electrodes.

Moreover, not all pulse energy at the focal spot is available to bubble formation (heating and liquid vaporization) and expansion, since part of the energy is used for plasma formation, that is liquid excitation and ionization. In effect, most of the energy seems to be used for plasma formation and only a small part is transferred to the bubble (cf. Section 3.3.1).

Exactly how much of the initial pulse energy that is transmitted to the bubble is difficult to say. A complicating fact was that some pulses gave rise to not one but several bubbles. To conclude, pulse energies given in this work are corrected with the factor of 0.64, but beware that this may not be the whole truth.

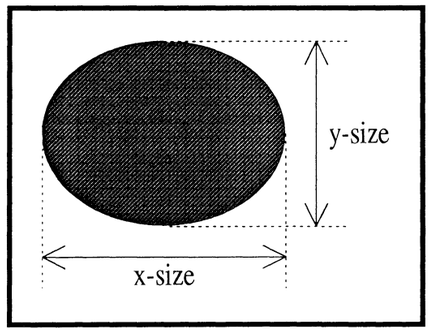

Figure 15. *Bubble size definitions.*

3.2 Bubble Size Measuring Method

As was earlier pointed out, the method to determine bubble size was as follows. For a specific IR-laser pulse energy and a certain delay time to the green laser pulse and the camera shot, ten bubble pictures were taken. According to the former description, all pictures were processed using PhotoFinish and Designer. The actual bubble size was determined inside Designer by using the tools Draw Ellipse and View Dimensions. Hence an ellipse was fitted to the biggest bubble in every picture and every bubble was given two size values, x-size value and y-size value, respectively (Figure 15). This method worked very well, although a small amount of

approximation was introduced now and then due to irregular bubble shapes, for example during collapse (Figure 16h). Since ellipses in Designer can be created in discrete sizes only, accuracies of 0.06 mm and 0.11 mm were allowed for, in x- and y-directions, respectively. Finally, an average value for the ten pictures was calculated and regarded as the bubble size for the given laser energy at the given moment of time. The reason not to measure bubble size manually with a ruler was that printing hard-copies of the pictures was too time-consuming.

3.3 Bubbles in Zero Electric Field

In the absence of an external electric field four picture series were taken, each with different laser pulse energy. Typical photographs of bubble expansion and contraction in transformer oil are shown in Figure 16 (all pictures presented throughout this work have been corrected for the interlacing effect, i. e. they have been stretched vertically with a factor of two). These events followed a laser pulse energy of 108 mJ, with the IR-laser pulse coming from the left. No filters were used and therefore the white area represents pure green laser light. Of course the green laser beam did not have an octagonal cross-section, but this was the shape of the aperture of the camera. Although all pictures in Figure 16 reveal only one bubble each, this was not always the case. Due to slightly different circumstances, for instance small variations in time duration and physical dimensions of the laser pulses, leading to more or less effective focusing, no liquid plasma looked the same from pulse to pulse. Most plasmas were short, thick and distinct, but a few of them were thinner and more elongated and sometimes gave rise to several, small bubbles instead of a big one.

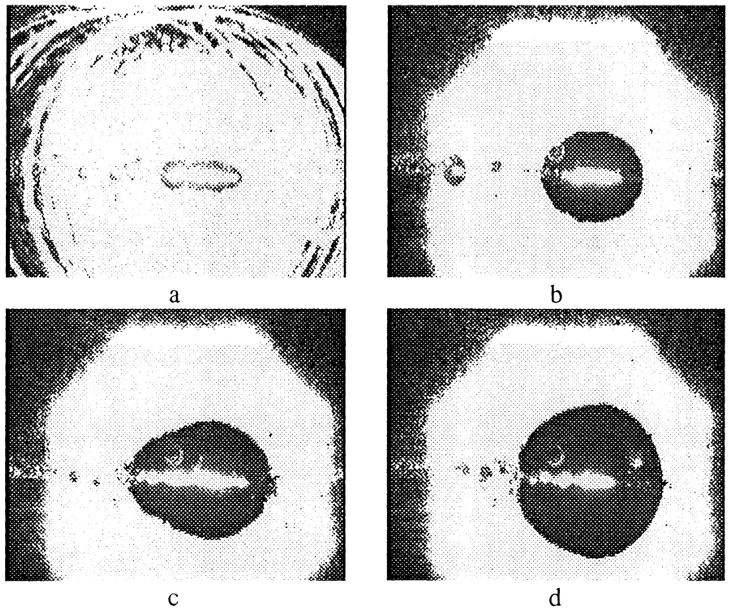

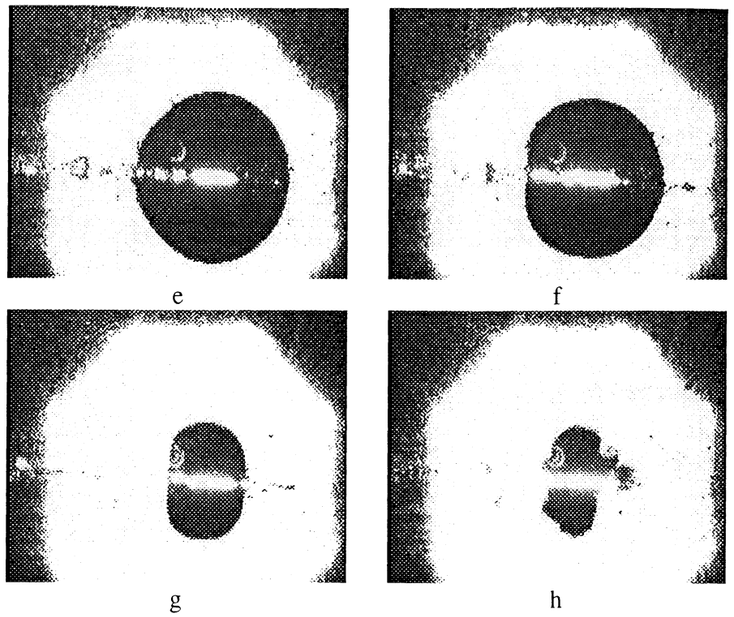

Figure 16. *Bubble growth following a 108 mJ laser pulse. Delay time (μs), bubble x-size (mm), and bubble y-size (mm): a) 2, 1.57, 0.54; b) 20, 1.98, 1.63; c) 40, 2.91, 2.07; d) 80, 2.79, 2.72; e) 120, 3.02, 3.04; f) 200, 2.62, 2.83; g) 250, 1.51, 2.07; h) 300, 1.74, 1.96. The last bubble picture illustrates how the bubble collapses and also the difficulty of determining its actual size owing to its non-elliptic shape.*

It can be seen that the bubbles are almost spherically shaped during expansion though initially slightly longer in the horizontal direction, which most probably is due to the fact that the IR-laser pulse propagates in this direction. Note also the radiated shock waves in the first picture. The pictures give support to those claiming that the spherical shape of a collapsing bubble is unstable [9]. Superimposed on the bubble is the original plasma light. Recall that the camera worked at an interlaced frequency of 50 Hz, thus having an exposure time of 0.02 seconds. Even if the whole plasma-bubble event is gone within a couple of hundred microseconds, the camera is sensitive to light for a much longer period of time and produces an integrated picture. In this way the plasma light is collected before the green laser light and both events can be observed, which can be regarded as an unexpected advantage of the slow camera.

Figure 17a-b present bubble size as a function of time in the case of a laser energy of 108 mJ. As already stated, every point corresponds to ten measurements. The bars represent one standard deviation up and one down*. Figure 17a shows the size in x-direction (along with the IR-laser pulse). The size in y-direction is shown in Figure 17b. In general, y-size data are probably

---

* The standard deviation σ for a Gaussian distribution can be estimated to be

$$\sigma = \sqrt{\frac{1}{n-1}\Sigma(x_i - m)^2}$$

where n = 10 is number of data points, x_i is data value, and m is the estimated expectation value. In this case m is equal to the arithmetic mean. The summation should be carried out for all n data points.

more reliable since energy is deposited mainly in the x-direction and therefore influences the x-size data, especially in the early stage of expansion and for high laser pulse energies.

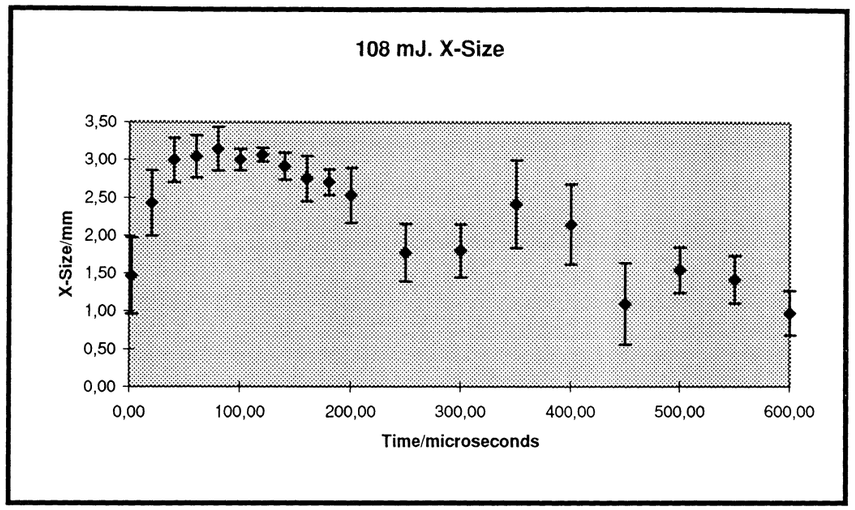

Figure 17a. *Bubble x-size as a function of time. Laser pulse energy: 108 mJ.*

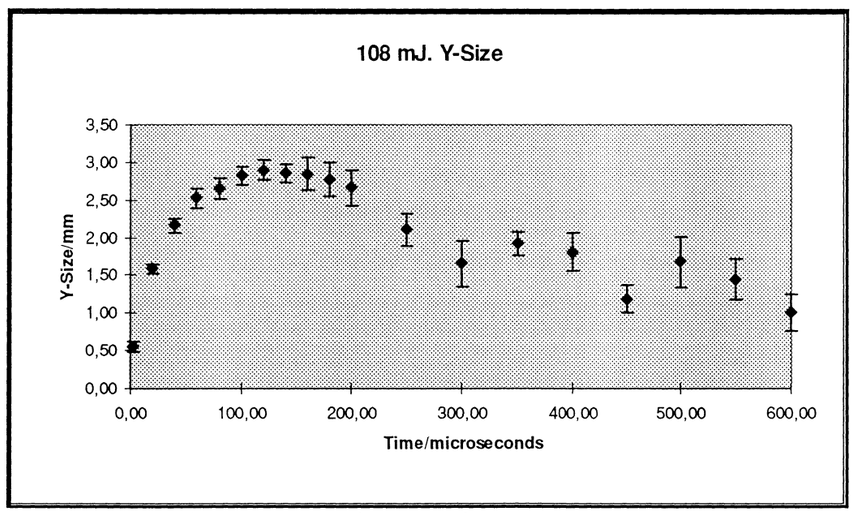

Figure 17b. *Bubble y-size as a function of time. Laser pulse energy: 108 mJ.*

From Figure 17 it is clear that the cavity expands for about 120 μs, which is the time for maximum bubble size. The contraction phase, which is also very distinct, lasts slightly longer than the expansion phase and collapse takes place shortly after 250 μs. The approximate symmetry about the time of maximum growth is apparent. The remaining pattern demonstrates rebounds. When the bubble collapses, its internal pressure rises in order to stop the collapse [3]. The expansion is then able to start over again. This kind of cavity growth is a well-known behaviour and can also be found when cavities are initiated by current pulses [3, 10]. The slope of the size versus time plot provides a measurement of cavity wall velocity, which decreases with time. For example, from Figure 17b the mean cavity wall velocity during the first 40 μs

can be estimated to be around 25 m/s. This is a reasonable figure with other similar results in mind [11].

3.3.1 Rayleigh model of cavitation

The expansion and collapse processes are well described by the Rayleigh model of cavitation [3, 6]. The energy to generate the high-pressure cavity and to provide for its rapid expansion is delivered by the laser pulse. Some of the laser pulse energy is converted into heat, which causes evaporation of the liquid and provides the driving force of expansion. In the process of expansion the cavity must do work against ambient pressure. The expansion is also limited by the inertia of the surrounding liquid [12], i. e. energy is lost due to the liquid viscosity. Cavity expansion goes on until the kinetic energy of the system (bubble and liquid) approaches zero, which occurs when the cavity wall velocity becomes zero. At this point the internal pressure is far below the ambient. Thus cavity expansion does not at all stop when internal pressure equals the ambient pressure.

Let us use the Rayleigh theory to derive an expression for the maximum radius of the expanded cavity and also an expression for its lifetime [3]. From the pictures above it is a good approximation to assume spherical cavity growth. In the early stage of bubble expansion it is possible to ignore the work done against ambient pressure and the bubble constitutes a constant kinetic energy system. For an incompressible fluid the following relation holds:

$$UR^2 = u(r) \cdot r^2, \qquad (1)$$

where R is cavity radius and U = dR/dt is cavity wall velocity. u is the liquid velocity and r can be thought of as radius vector with r = 0 in the centre of the cavity. The meaning of Equation 1 becomes clearer if one notes that it has the dimension of flux (m^3/s). Thus

$$u(r) = \frac{UR^2}{r^2} \qquad (2)$$

and the kinetic energy E of the fluid surrounding the cavity becomes

$$E = \frac{\rho}{2}\int_R^\infty u^2(r) \cdot 4\pi r^2 \, dr = \frac{\rho}{2}\int_R^\infty \frac{U^2R^4}{r^4} \cdot 4\pi r^2 \, dr = 2\pi\rho U^2 R^3 \qquad (3)$$

with ρ denoting the density of the liquid. If the kinetic energy of the system is constant E_0, then

$$U^2 = \left(\frac{dR}{dt}\right)^2 = \frac{E_0}{2\pi\rho R^3} \qquad (4)$$

since the work against ambient pressure is ignored. Integration gives cavity radius as a function of time:

$$R(t) = \left(\frac{5}{2} \cdot \left(\frac{E_0}{2\pi\rho}\right)^{1/2} \cdot t\right)^{2/5} + R_0 \approx \left(\frac{E_0}{\rho}\right)^{1/5} \cdot t^{2/5}. \qquad (5)$$

The validity of this relation can be verified from the expansion phase data in Figure 17. Figure 18 shows 2R versus $t^{2/5}$ for $t \leq 60$ µs and confirms this simple Rayleigh model of early expansion.

As the bubble expands, it does work against the ambient pressure p_a. To take this into account, the energy balance equation for the system with initial kinetic energy E_0 can be written as

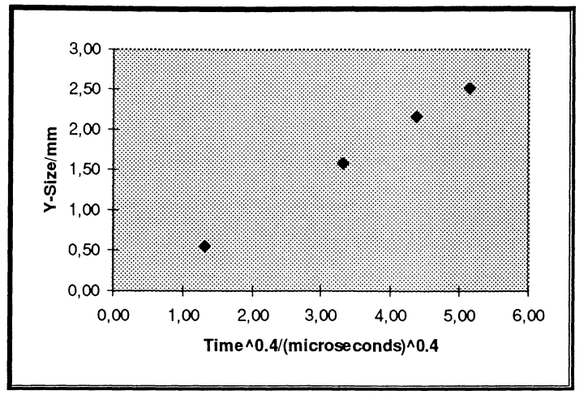

Figure 18. *Early expansion. Bubble y-size vs. $t^{2/5}$. Laser pulse energy: 108 mJ.*

$$E_0 = 2\pi\rho U^2R^3 + p_aV = 2\pi\rho U^2R^3 + p_a \cdot \frac{4}{3}\pi R^3, \qquad (6)$$

where the second term describes the work against the ambient pressure since V denotes bubble volume. Surface tension is neglected. Solving for U^2 gives

$$U^2 = \frac{E_0}{2\pi\rho R^3} - \frac{2p_a}{3\rho}. \qquad (7)$$

The maximum radius R_{max} is obtained for U = 0. Thus

$$R_{max} = \left(\frac{3E_0}{4\pi p_a}\right)^{1/3}. \qquad (8)$$

This relation will be examined further later on, but we can immediately conclude that E_0 not is equal to the laser pulse energy at the focal spot. For the case above, with p_a = 101 kPa and E_0 = 108 mJ, we get a maximum radius of 6.34 mm, which is to be compared with half the maximum y-size in Figure 17b, i. e. 1.45 mm. For the theoretical maximum radius to coincide with the experimental one, an expansion energy of E_0 = 1.3 mJ would be sufficient. As in the case of initiation by current pulses [10], most of the injected laser pulse energy is used to evaporate the liquid. Only about one percent of the energy is transferred to the bubble, which is in consistence with what others have found [3]. This amount of energy is small not only compared with the laser pulse energy, but also compared with how much of the pulse energy that is at all transferred to the liquid. From calorimetric measurements, the amount needed for plasma formation is approximately 20-30 mJ [2].

The cavity expansion terminates when the kinetic energy of the system passes through zero. At this point, when the cavity radius has reached its maximum value, the internal pressure is far below the ambient, which causes the cavity to collapse. Equating the ambient pressure work W_a, when expanding from R to R_{max},

$$W_a = \frac{4}{3}\pi p_a \cdot (R_{max}^3 - R^3), \qquad (9)$$

to the kinetic energy of the fluid, Equation 3, gives

$$U^2R^3 = \frac{2p_a}{3\rho} \cdot (R_{max}^3 - R^3) \qquad (10)$$

from which it follows that

$$U(R) = \sqrt{\frac{2p_a \cdot (R_{max}^3 - R^3)}{3\rho R^3}}. \qquad (11)$$

The time τ it will take for the cavity to collapse can be calculated from Equation 11 through integration:

$$\tau = \int_0^{R_{max}} \frac{dR}{U(R)} = R_{max} \cdot \sqrt{\frac{\rho}{6p_a}} \cdot \frac{\Gamma(5/6) \cdot \Gamma(1/2)}{\Gamma(4/3)} = 0.915 \cdot R_{max} \cdot \sqrt{\frac{\rho}{p_a}}, \qquad (12)$$

where $\Gamma(x)$ is the gamma function. Using Equation 8 this can be written as

$$\tau = 0.915 \cdot \left(\frac{3E_0}{4\pi p_a}\right)^{1/3} \cdot \sqrt{\frac{\rho}{p_a}} \qquad (13)$$

Due to symmetry, τ not only gives the time to collapse, but also the time for cavity expansion. Therefore the bubble lifetime is 2τ. What do the experimental data shown in Figure 17 say about this? According to Figure 17b, R_{max} is equal to 1.45 mm. The density of transformer oil is ρ = 860 kg/m^3. Putting p_a = 101 kPa gives τ = 122 µs, which agrees well with the time for expansion found from experiment.

3.3.2 Additional experimental results

Both bubbles in Figure 19 have been initiated by a laser pulse energy of 48 mJ. The picture in Figure 19a was taken 20 µs after initiation and should be compared with the bubble in Figure 16b. The delay time in Figure 19b is 120 µs and thus the same as in Figure 16e. For the human eye the differences may not be too obvious, but the 48 mJ bubbles are actually smaller than those initiated by 108 mJ. From Equations 5 and 8 this is what we expected. In analogy with Figure 17, Figure 20a-b illustrate bubble growth in the case of a laser pulse energy of 48 mJ (note the different scale). The most striking feature with these plots in comparison with the previous ones is the considerable scatter in the data. This is most certainly due to the lower laser pulse energy. At lower laser pulse energies, the pulse to pulse energy variation increases. Still, the phases of expansion, collapse, and rebounds are evident and clear.

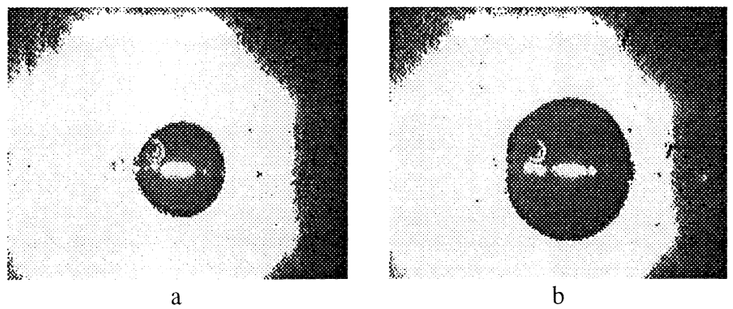

a b

Figure 19. *Bubble growth following a 48 mJ laser pulse. Delay time (µs), bubble x-size (mm), and bubble y-size (mm): a) 20, 1.74, 1.63; b) 120, 2.56, 2.39.*

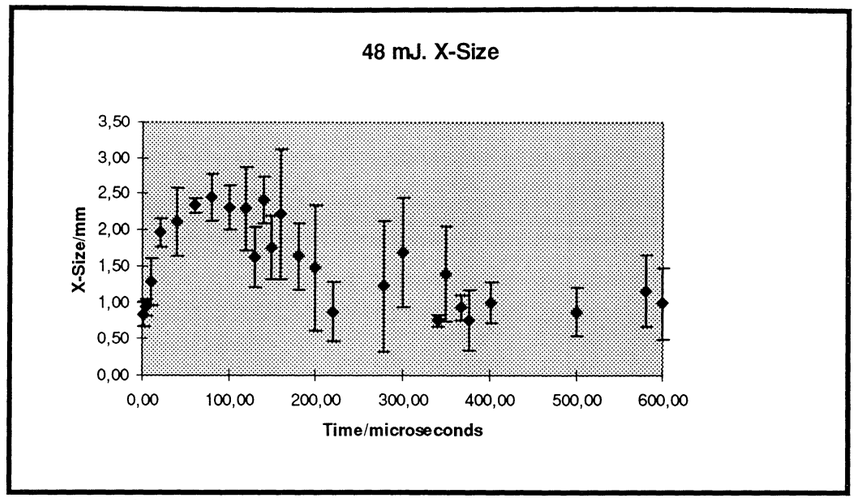

Figure 20a. *Bubble x-size as a function of time. Laser pulse energy: 48 mJ.*

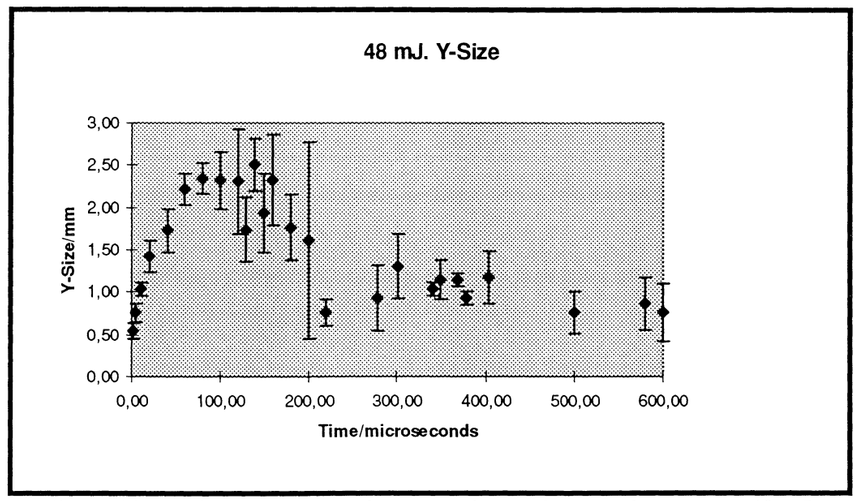

Figure 20b. *Bubble y-size as a function of time. Laser pulse energy: 48 mJ.*

Before being concerned about bubble maximum radius and bubble lifetime, let us first take a look at the remaining data representing laser pulse energies of 22 mJ and 77 mJ. Figure 21a-b present the most obscure data collection suffering from a scatter even greater than that in Figure 20a-b. The laser pulse energy is 22 mJ. At last, to restore order, Figure 22a-b show bubble size development caused by a 77 mJ laser pulse. At this energy level, a bubble can look like the one shown in Figure 23. In Figure 24 a bubble collapse has been captured.

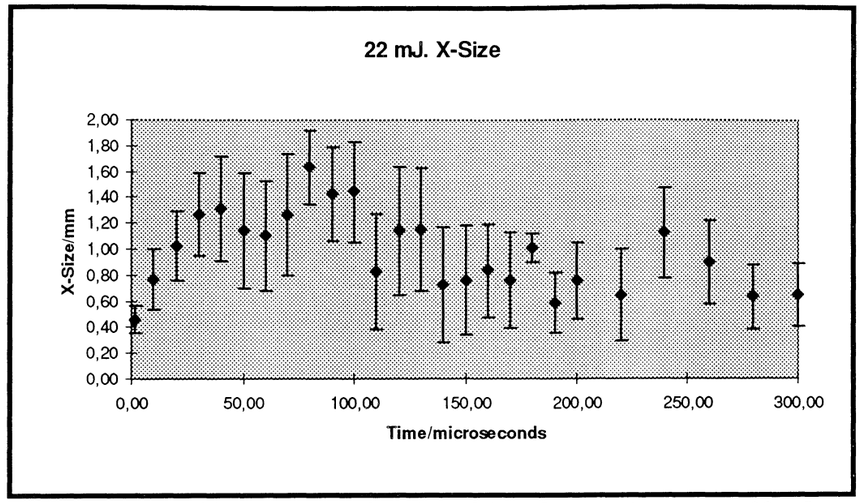

Figure 21a. *Bubble x-size as a function of time. Laser pulse energy: 22 mJ.*

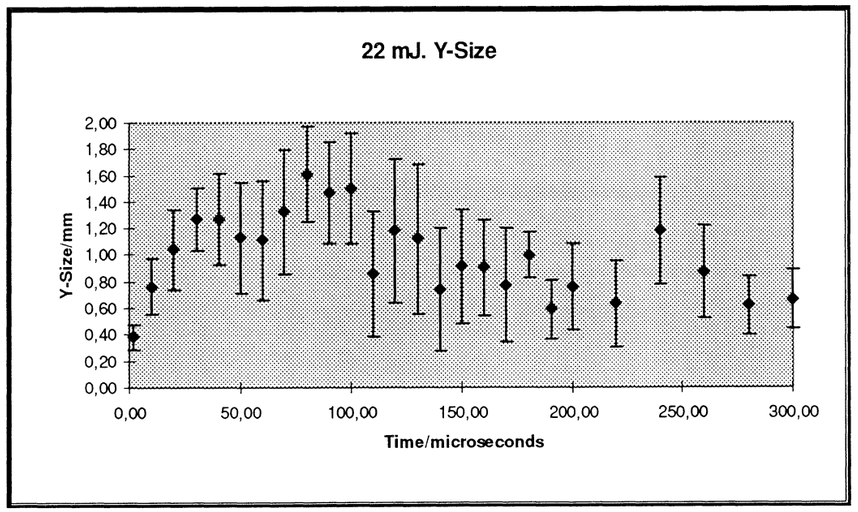

Figure 21b. *Bubble y-size as a function of time. Laser pulse energy: 22 mJ.*

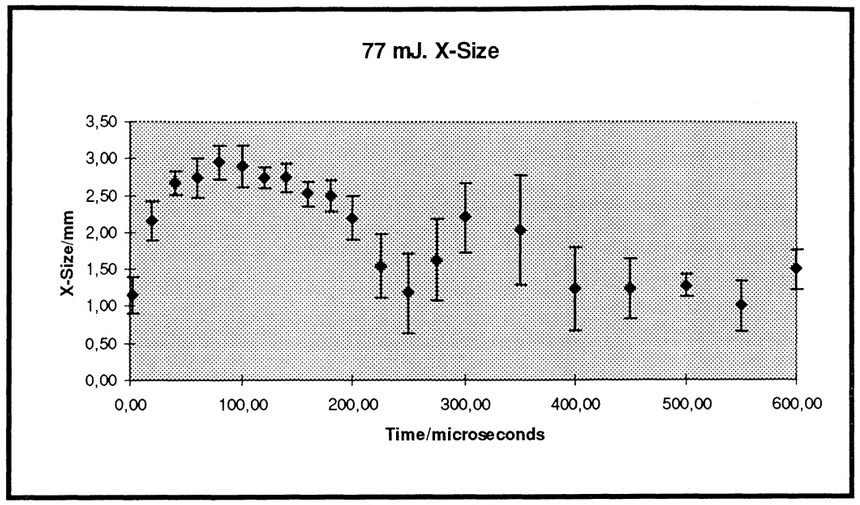

Figure 22a. *Bubble x-size as a function of time. Laser pulse energy: 77 mJ.*

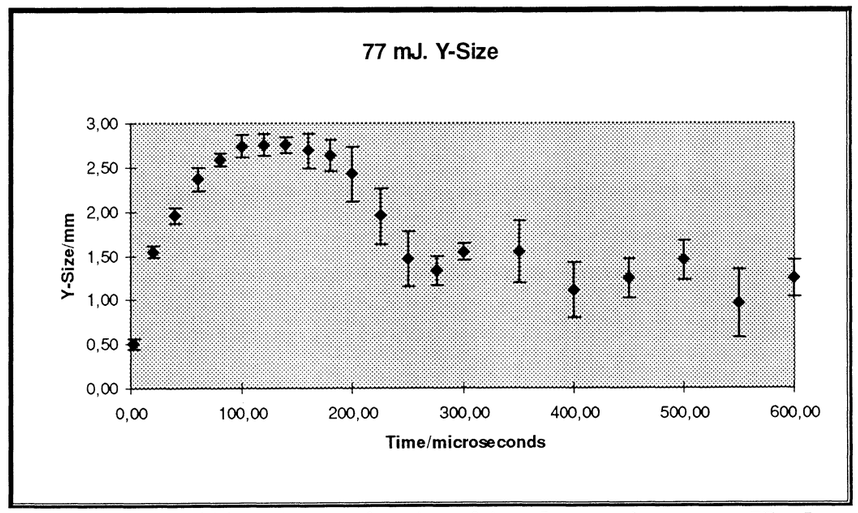

Figure 22b. *Bubble y-size as a function of time. Laser pulse energy: 77 mJ.*

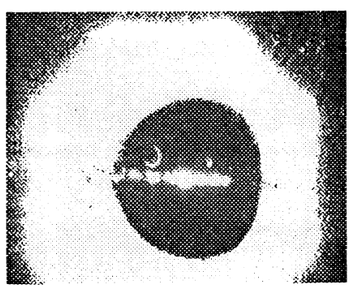

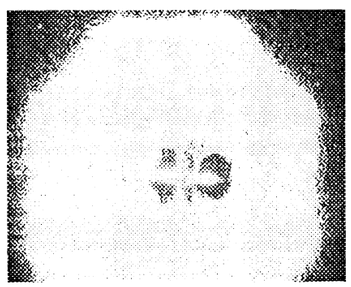

Figure 23 (left). *Example of bubble appearance at a delay time of 120 μs for a laser pulse energy of 77 mJ. Bubble x-size: 2.85 mm. Bubble y-size: 2.83 mm.*

Figure 24 (right). *A bubble, initiated by a laser pulse energy of 77 mJ, collapses after 400 μs. The bubble to the right still lives. Its x-size is 0.58 mm and its y-size is 0.98 mm.*

According to Equation 8, the maximum bubble radius R_{max} is proportional to $E_0^{1/3}$. To test this relation, the following plot (Figure 25) shows maximum bubble size versus $E_0^{1/3}$ for the energies 22 mJ, 48 mJ, 77 mJ, and 108 mJ. Maximum x-size as well as maximum y-size is plotted. The values, which are presented in Table 1 below, are taken directly from the figures above without any curves having been fitted to the data points. From Figure 25 it is not so easy to tell if the relation is linear or not, but possibly it is.

E_0/mJ	$E_0^{1/3}/(mJ)^{1/3}$	Max. x-size/mm	Max. y-size/mm
22	2.80	1.63 (0.29)	1.61 (0.36)
48	3.63	2.45 (0.33)	2.51 (0.31)
77	4.25	2.95 (0.23)	2.75 (0.11)
108	4.76	3.14 (0.29)	2.90 (0.13)

Table 1. *Maximum bubble size as a function of energy. Figures in brackets indicate standard deviation.*

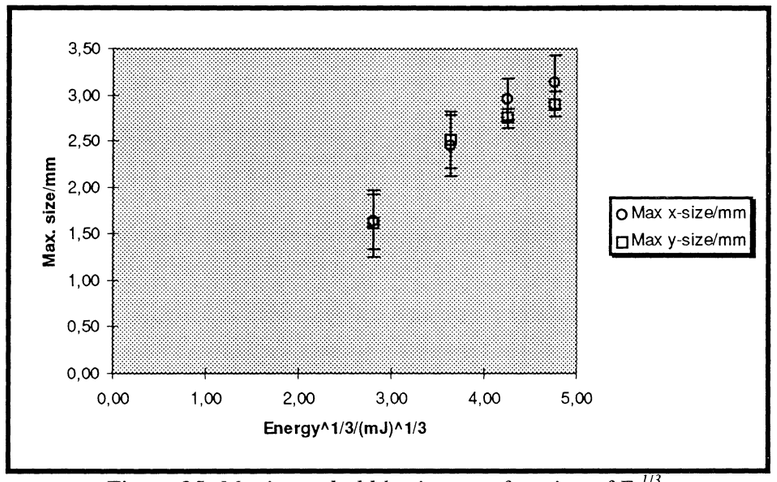

Figure 25. *Maximum bubble size as a function of* $E_0^{1/3}$.

Equation 12 states that bubble time of expansion τ is directly proportional to maximum bubble radius R_{max}. This relation is tested in Figure 26, with plotted values given in Table 2. Experimental values have been estimated from Figure 17b, 20b, 21b, and 22b, respectively. As before, oil density was set to $\rho = 860$ kg/m^3. Equally, ambient pressure p_a was set to 101 kPa. It is clear from Figure 26 that Equation 12 seems to hold.

E_0/mJ	Max. y-size/mm	τ_{exp}/μs	τ_{th}/μs
22	1.61 (0.36)	80	68
48	2.51 (0.31)	110	106
77	2.75 (0.11)	120	116
108	2.90 (0.13)	130	122

Table 2. *Maximum bubble y-size and corresponding time of expansion (exp = experimental estimation, th = theoretical value calculated from Equation 12).*

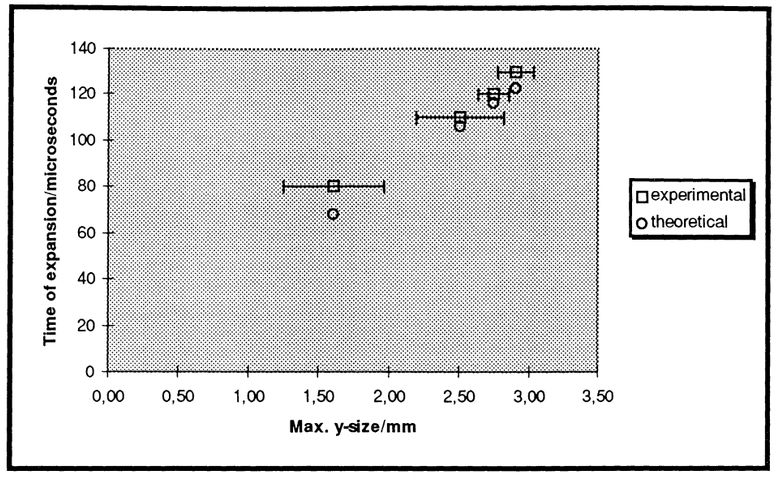

Figure 26. *Bubble time of expansion as a function of maximum bubble y-radius.*

3.4 BUBBLES SUBJECTED TO AN ELECTRIC FIELD

A few minor problems preceded the studies concerning bubble appearance in an electric field. It got increasingly difficult to produce distinct plasmas no matter which laser pulse energy was used. In the eagerness to enhance plasma quality, the entrance window of the test cell was destroyed. The IR-laser pulse burnt a hole straight through the glass. The last focusing lens was also damaged, so it was replaced as well. Trying to get more power out of the IR-laser, the oscillator flashlamps were replaced. In addition, the gold reflectors surrounding the YAG crystals (there were one crystal in the oscillator part of the laser and one crystal in the amplifier part) were cleaned. These actions nearly doubled the oscillator output of the laser. Before it was possible to proceed with the measurements, however, the transformer oil had to be filtered from impurities. To conclude, these measures all led to the fact that it no longer was possible to accurately compare previously found bubble sizes – when no external electric field was applied – with bubbles to be initiated with the new set-up. Nevertheless, this situation would have been hard to avoid, since the focal spot had to be repositioned anyway (cf. Section 3.1). To somehow compensate for this, a minor series of bubble pictures was taken, half of it with an electric field present and half of it without. This will be dealt with in Section 3.4.4.

3.4.1 Prebreakdown processes revisited

Several prebreakdown processes have been proposed. The first two that one can think of don't even involve streamers. Is it possible for the cavity to expand so much that it will be able to bridge the entire electrode gap and thus on its own cause electric breakdown? According to cavity wall velocity this proposal cannot explain breakdown for larger (> 2 mm) gaps due to small time lags from initiation to breakdown [6]. What if the bubble expands normally in the beginning of the process and thereafter elongates in the field direction? Another possibility is for the bubble to grow until an electrohydrodynamic instability develops at its surface, causing the initiation and propagation of a streamer [3, 12, 13]. If so, will this instability be of macroscopic, visible size? Will there be more than one? Another, fourth model was put forward by

Sunesson et al. [2]. Their idea is that gas discharges (partial discharges) inside the expanding vapour cavity will create free charges, which will migrate to the surface of the cavity. Cavity elongation in the field direction will then develop because of present electrostatic forces. Finally, after a number of discharges, a streamer will originate from the elongation. Proof of gas discharges is based upon analysis of current and light measurements [6, 14, 15].

Of primary interest with the electric field bubble studies in this section was the question whether the bubble became elongated in an electric field. After initial cavity expansion but before streamer initiation, does the bubble in any way stretch due to the electric field?

3.4.2 Bubble stability in an electric field

According to existing theory [16, 17], a compressible bubble (gas bubble) immersed in a liquid medium and subjected to a uniform electric field will elongate in the direction of the field whenever the permittivity of the bubble differs from the permittivity of the liquid. An initially spherical bubble will distort and take the shape of an ellipsoid. If space charge is present or if the bubble is situated close to an electrode, the deformation of the bubble will be asymmetric [17]. It has been shown [16] that the permittivity ratio $q = \varepsilon_{bubble}/\varepsilon_{liquid}$ is of crucial importance. A non-conducting bubble for which $q < 20$ has a stable shape at all values of the electric field. This means that the ratio of the major to minor semi-axis, here denoted γ, not will change very much as the field strength is increased. A conducting bubble, or a non-conducting bubble with $q \geq 20$, has a critical stable shape for a certain value of the electric field, corresponding to a critical value of γ. A field increase at this point will cause γ to rise abruptly, i. e. the bubble will strongly elongate, get unstable, and eventually dissipate. In our case we deal with transformer oil and two questions have decisive significance: a) is the transformer oil bubble a conducting or a non-conducting bubble? and b) if it is non-conducting, what is the permittivity of it? Most gases have a relative permittivity near 1, and since the relative permittivity of transformer oil is 2.4, this implies that $q \approx 0.4$. In this case, referring to Garton and Krasucki [16], a non-conducting bubble in a field as strong as 50 MV/m would not elongate noticeably.

3.4.3 Picture timing

Before presenting the first pictures of bubbles in an electric field, it is a good idea to say something about timing. There was no way to trigger the green laser in such a way that it would have been possible to choose to image a specific step in the breakdown process. In other words, it was not possible to let some prebreakdown current (streamer currents precede breakdown) trigger the green laser, which had a pulse delivering time exceeding 300 μs (the entire breakdown process only exists for about 10 μs). Further, time from initiation to breakdown varied from 70 μs up to 110 μs from one process to the next, and the only variable to play with was the delay time of the green laser relative to the time of initiation. Thus it was a question of luck to get pictures of specific steps in the breakdown process, for example pictures showing streamer propagation. Not using too low a voltage level helped to keep the spread of time to breakdown low.

3.4.4 Experimental results and the first streamer glimpses

Bubbles were initiated at the centre of the electrode gap by laser pulses reaching a pulse energy of 86 mJ. The electrode gap length was 4.1 mm, and a high voltage of +50 kV was applied to the upper electrode giving an electric field intensity of approximately 12 MV/m in the middle of the gap. Gap length was chosen with respect to camera size as well as breakdown voltage level. No attenuation filter was needed, but light from streamers and breakdown arcs demanded an interference filter before the camera. Without the interference filter important parts of the shadow objects would have been invisible, since light from the breakdown process would have covered the shadow picture.

Initially, a little more than 100 pictures were taken. For every ten pictures, delay time was increased by 10 µs. Thus the first ten pictures were taken at a delay time of 10 µs while the next ten pictures were taken at a delay of 20 µs, and so on. Figure 27 shows one of the first pictures taken. There are two bubbles in the middle and the electrodes can be seen in the top and bottom parts of the picture. The dark area under the left bubble is due to the interference filter, while the total dark to the left is up to a non-perfect alignment of the camera and the green laser beam. The picture was taken 40 µs after initiation and 48 µs prior to breakdown. No streamers can be seen at this early stage, nor is it possible to observe any bubble elongation in the direction of the field. A similar picture is shown in Figure 28, although this picture was taken with a longer delay time: 70 µs after initiation and 10 µs prior to breakdown. Neither this bubble seems to be elongated. Its shape is comparable with bubbles not subjected to an electric field. Exact sizes will be discussed later. At the moment we are first of all interested in bubble shape characteristics.

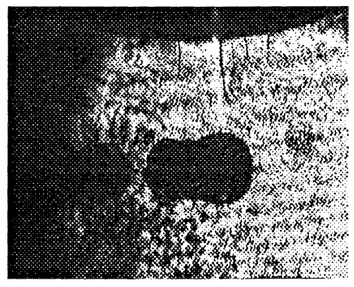

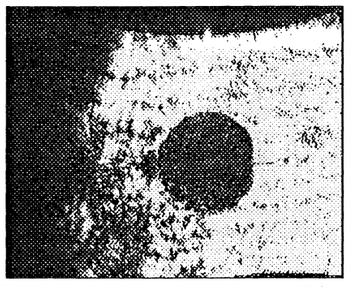

Figure 27 (left). *Bubbles in an electric field (12 MV/m). Laser pulse energy: 86 mJ. Time: 40 µs. Time left to breakdown: 48 µs. The bubble to the right has an x-size of 2.09 mm and a y-size of 1.09 mm.*
Figure 28 (right). *Bubble in an electric field (12 MV/m). Laser pulse energy: 86 mJ. Time: 70 µs. Time left to breakdown: 10 µs. Bubble x-size: 1.86 mm. Bubble y-size: 1.85 mm.*

Figure 29 is exciting. It is the first picture revealing negative streamers. Like fingers they grow from the top of the bubble and reach for the positive electrode. The picture was taken only 1 µs before breakdown, which this time occurred 71 µs after initiation. Still no macroscopic elongation of the bubble can be seen, not even around the streamer initiation points. The shadows below the bubble to the right probably come from positive streamers forming something like a streamer delta outside the ground electrode. They are too narrow to be seen in the area close to the bubble. Typical negative streamers are also shown in Figure 30.

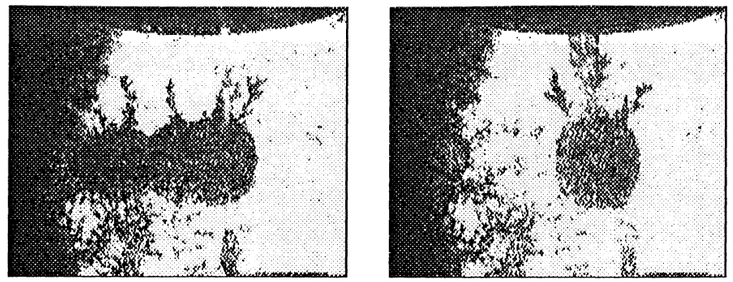

Figure 29 (left). *Bubble (probably a union of two cavities) and negative streamers in an electric field (12 MV/m). Laser pulse energy: 86 mJ. Time: 70 µs. Time left to breakdown: 1 µs. Bubble x-size: 3.49 mm. Bubble y-size: 1.41 mm. Are the shadows near the ground electrode caused by positive streamers?*
Figure 30 (right). *Typical negative streamers. Time: 100 µs, 20 µs after breakdown. Bubble x-size: 1.63 mm. Bubble y-size: 1.74 mm.*

Figure 31 has got it all. Breakdown took place 66 µs after initiation. The picture was taken 4 µs later. Negative streamers are apparent as well as the breakdown arc. Shadows near the ground electrode, outside the breakdown arc, indicate positive streamers. One might think that bubble elongation is present in this picture, but my suggestion is that the bubble is bigger to the right than to the left due to focusing effects rather than the electric field.

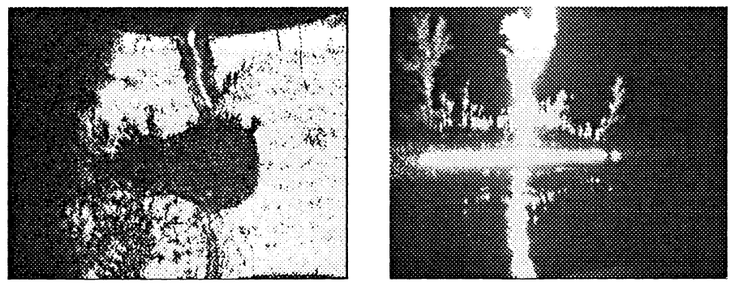

Figure 31 (left). *Negative streamers and breakdown arc. Possible positive streamers between bubble and ground electrode. Time: 70 µs, 4 µs after breakdown. The bubble is most certainly a union of two cavities. Bubble x-size: 2.79 mm. Bubble y-size: 1.63 mm.*
Figure 32 (right). *Breakdown picture without use of green laser light. Time: 80 µs. Time left to breakdown: 40 µs.*

Figure 32 is special. This picture was taken without use of the green laser. All light comes from the breakdown process itself. Breakdown occurred 120 µs after initiation and the camera opened up 40 µs earlier (recall the integration effect). Not only the negative streamers and the breakdown arc are apparent in the picture, but also the bubble.

To confirm the question of no elongation in an electric field, the picture series above was later supplemented by another 40 pictures. First, 20 pictures were shot without any field applied to the gap. Then, other things being equal, the rest of the pictures were shot with +40 kV applied to the upper electrode giving an electric field intensity of 8.5 MV/m since the gap length now was 4.7 mm. The laser pulse initiation energy was 63 mJ and the green laser delay was set to

80 μs. As before, the focal point was at the centre of the gap. An attenuation filter was used, but since the low electric field intensity rarely caused breakdown, no interference filter was needed and this gave rise to sharper pictures since the pictures no longer suffered from the interference pattern of the filter. Figure 33 shows an example of a bubble without the field present. In Figure 34, on the other hand, a bubble subjected to the field is shown. Table 3 summarizes what was found. Even though the bubble size in the direction of the field (y-size) was slightly increased when the field was introduced, the size in the direction perpendicular to the field (x-size) was also increased. The result is that no elongation can be seen. In addition, the small increase of size is far below the standard deviation. Therefore, neither bubble elongation nor bubble growth due to the electric field can be verified.

	Without field	With field
Average x-size/mm	2.20 (0.21)	2.24 (0.21)
Average y-size/mm	2.23 (0.15)	2.28 (0.13)
Average size ratio, y/x	1.02 (0.06)	1.03 (0.08)

Table 3. *Results of elongation measurements. The size ratio can be compared with γ (cf. Section 3.4.2). Figures in brackets indicate standard deviation.*

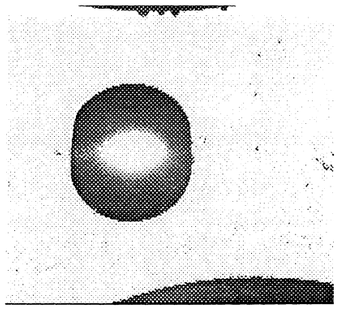

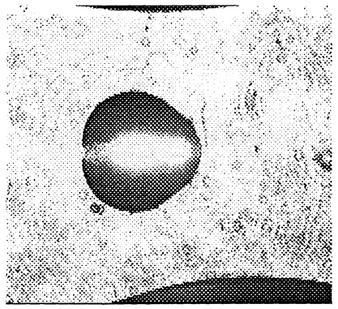

Figure 33 (left). *Bubble not subjected to an electric field. Laser pulse energy: 63 mJ. Time: 80 μs. Bubble x-size: 2.33 mm. Bubble y-size: 2.39 mm.*
Figure 34 (right). *Bubble subjected to an electric field (8.5 MV/m). Laser pulse energy: 63 mJ. Time: 80 μs. Bubble x-size: 2.33 mm. Bubble y-size: 2.17 mm.*

3.5 Conclusion

The studies of gas bubbles in this chapter lead to the conclusion that bubble growth follows the Rayleigh model of cavitation, also when the bubbles are subjected to an electric field. No macroscopic change of size due to such a field can be verified. Time scale can be a reason for this. The bubble expansion phase exists only for about 100 μs. Compare with a water droplet in silicon oil subjected to an electric field of 1 MV/m, which needs approximately 10 ms before a macroscopic deformation can be seen [17]. Therefore, the driving force for bubble expansion seems to be totally provided by the vapour pressure. The bubble growth goes on until some kind of microscopic instability occurs and streamers are initiated. It is hard to believe that the bubble is non-conducting since it originates from a plasma. If one assumes a plasma charge density of 10^{21} electrons per cm^3 [2] and a plasma size of 2 mm × 50 μm × 50 μm = $5 \cdot 10^{-6}$

cm^3 the total charge Q becomes $5 \cdot 10^{-6} \cdot 10^{21} \cdot 1.6 \cdot 10^{-19}$ As = $8 \cdot 10^{-4}$ As. An electric field E = 10 MV/m then gives a total electrostatic force F = QE = $8 \cdot 10^3$ N if the bubble charge is equal to the charge of the plasma. The field thus gives the bubble an acceleration of a = F/m = $8 \cdot 10^6$ m/s^2 for a gas mass of m = $1 \cdot 10^{-3}$ kg. This acceleration can be compared with the bubble growth acceleration in the case of zero electric field. Previously, the cavity wall velocity was estimated to be 25 m/s during the first 40 µs. This gives an acceleration of $6 \cdot 10^5$ m/s^2. From this calculation it is evident that the electric field would have a great influence on bubble growth, but the assumption of plasma charge density is uncertain. The electrostatic acceleration gives a growth of $8 \cdot 10^6 \cdot (100 \cdot 10^{-6})^2/2$ m = 40 mm in 100 µs, which is unreasonable since such a growth has not been observed. The ionization level in the bubble is probably lower than in the plasma.

4. Prebreakdown Streamers

4.1 Streamer Initiation and Propagation

A so-called electrohydrodynamic instability of the cavity wall has been proposed to be the source of negative streamers [18]. The electric field will act on charges at the cavity/fluid interface and cause instabilities to grow exponentially in time. As the amplitude of an instability increases, the cavity wall structure evolves into finger-like channels originating from the ionized vapour cavity. Thus negative streamers can be thought of as columns of ionized gas being dragged through the fluid by the electrostatic force. However, far from all instabilities develop into streamers.

For positive streamers the electric field will be concentrated at the streamer tip leading to liquid ionization in this region. Streamer propagation due to the electrostatic force will take place. A positive streamer tip will attract free electrons in the liquid. These electrons will leave positive ions in front of the tip and give rise to a continuous current [5, 6]. In this way the positive streamer will be extended throughout the ionized volume. The positive streamer propagation continues in this manner.

Negative streamers propagate through successive discharges, which are observed in prebreakdown current measurements [5, 6]. The propagation speed of positive streamers, 1-10 km/s, is a factor of ten higher than for negative streamers. A reason for this is that the liquid at the positive streamer tip is ionized directly without going through the vapour phase [5].

Good examples of streamers are shown in Figure 35. Note the filamentary positive streamers below the bubble. They are as narrow as threads compared with the thicker, bush-like negative streamers. +55 kV was applied to the gap with length 4.7 mm yielding an electric field intensity of 12 MV/m. The laser pulse initiation energy was 80 mJ. An attenuation filter (10% transmission) as well as an interference filter was used for the green laser light. The picture was taken 80 μs after the IR-laser pulse hit the liquid. Breakdown occurred 57 μs after initiation and according to breakdown current measurements (giving the same kind of curves as studied by Bäckman [6]) the first positive streamer was initiated 4 μs before breakdown. Figure 36 gives more streamer examples and in Figure 37 the positive streamer filamentary branches near the ground electrode are clearly seen.

The broad, bush-like negative streamers in Figure 35 have a minimum diameter of approximately 200 μm, but this figure most certainly represents several streamer channels. In Figure 36, where the negative streamers look almost perfect regarding the bush-like propagation pattern, their root diameter is about 100 μm. The positive streamer channels seen in Figure 35 have a diameter of 30 μm.

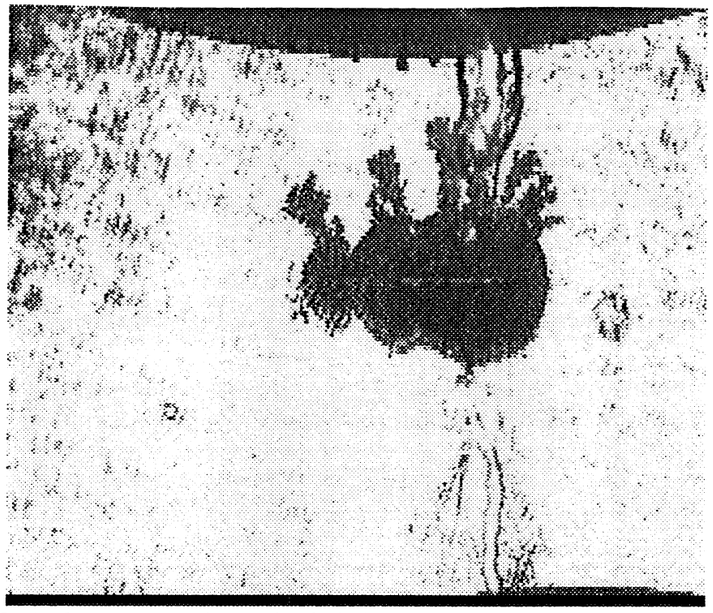

Figure 35. *Typical negative (above the bubble, near the positive electrode) and positive (below the bubble, close to the ground electrode) streamers. Electric field intensity: 12 MV/m. Laser pulse initiation energy: 80 mJ. Time: 80 μs after plasma initiation and 23 μs after breakdown. The first positive streamer connected 53 μs after plasma initiation and 4 μs before breakdown.*

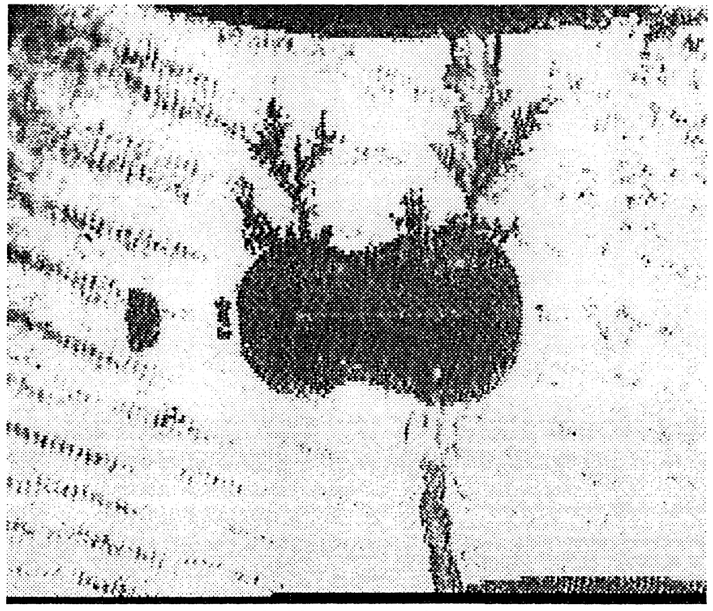

Figure 36. *More streamers. Electric field intensity: 12 MV/m. Laser pulse initiation energy: 80 mJ. Time: 81 μs after plasma initiation and almost simultaneous with breakdown. The first positive streamer connected 71 μs after plasma initiation, i. e. 10 μs before breakdown.*

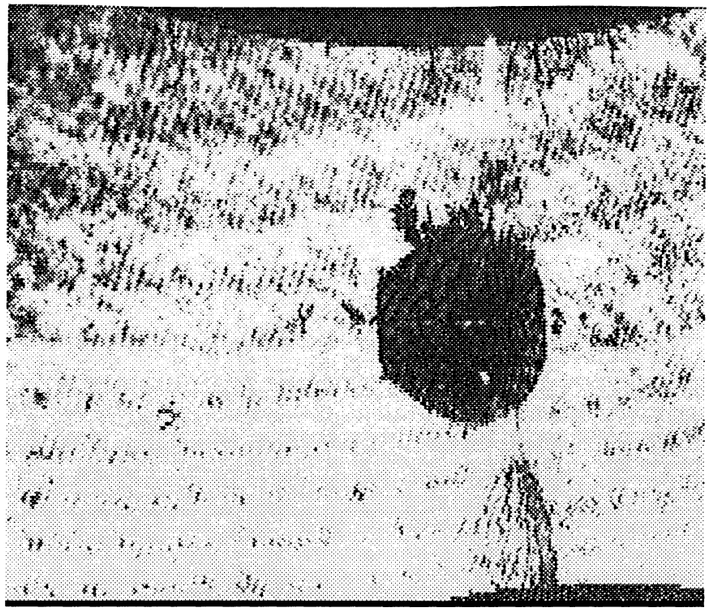

Figure 37. *Nice example of positive streamer branching. Note that the negative streamers not yet have reached the positive electrode. Breakdown is about to happen within 4 μs and the picture was taken 82 μs after plasma initiation. The first positive streamer connected 5 μs prior to this photograph. Electric field intensity: 12 MV/m. Laser pulse initiation energy: 80 mJ.*

4.2 Propagation Speed of Negative Streamers

From situations like the one shown in Figure 37 there is a possibility to estimate the propagation speed of negative streamers. Knowing how much time Δt there is left to breakdown, the speed v is given by $v = \Delta x/\Delta t$, where the distance Δx to the electrode can be measured from the picture [1]. For a given voltage, the propagation speed is relatively constant as the streamer crosses the gap. Streamer velocity is also weakly viscosity dependent [12]. For negative point/plane gaps the following expression for streamer propagation speed has been arrived at [12]:

$$v = \left(\sqrt{\pi} \frac{\varepsilon U^2}{4\rho \sqrt{\nu L R a}} \right)^{2/3}, \qquad (14)$$

with ε denoting permittivity, U voltage, ρ liquid density, ν liquid viscosity, L streamer length, R streamer radius, and a tip/plane spacing.

To deduce a value for the speed of negative streamers propagating in an electric field intensity of 11 MV/m ten suitable pictures were used. Every such picture had to be clear with distinct position of the negative streamer tip. In case the breakdown arc was visible, Δx was assumed to follow the path of the arc. If the breakdown arc did not exist, Δx was approximated to be the shortest distance between the streamer tip and the nearest electrode. Note that this not necessarily represents the real propagation path of the streamer. Calculations lead to a propa-

gation speed mean value of 239 m/s with a standard deviation as big as 127 m/s. For these ten situations, maximum speed was found to be 544 m/s, while minimum speed was 110 m/s. The result is in accordance with what others have found [12].

No data was available for the calculation of the propagation speed of positive streamers, i. e. there were no pictures revealing positive streamers in situations by analogy with the negative streamer situation in Figure 37. Particularly, the positive streamers were too fast and their tip positions were difficult to determine with any certainty. However, there is no doubt that they are several factors faster than their negative colleagues.

4.3 Effect of Electrode Polarity and Focal Spot Position on the Breakdown Process

So far we have only been concerned with prebreakdown processes with positive high voltages applied to the gap and with initiation laser pulses focused at the centre of the gap. In this case, when the vapour bubble is created in the middle of the electrode gap, the first connecting streamer is a positive one, which connects the bubble to the ground electrode and makes the bubble equipotential. Negative streamers bridge the rest of the gap, starting from the bubble and reaching for the high voltage electrode. Regarding gap polarity and focal spot position, there are four other cases to study:

a) focal spot close to the ground electrode and positive high voltage,
b) focal spot close to the ground electrode and negative high voltage,
c) focal spot close to the high voltage electrode and positive high voltage,
and
d) focal spot close to the high voltage electrode and negative high voltage.

These cases have also been studied by Bäckman [6], who measured prebreakdown currents and streamer light emission. In addition to the pictures, the same kind of prebreakdown current measurements were used in this work in order to make the studies safer and more complete. An example is given in Figure 38. Occasional pulses due to gas discharges in the bubble can be seen to the left. The large pulse preceding breakdown is caused by the first connecting positive streamer and is followed by pulses generated by negative streamer propagation. It has been found [6] that the time to the large pulse has a maximum when the focal spot is placed in the middle of the gap, no matter gap polarity. This is not too difficult to understand, since the distance from the cavity wall to the electrodes has a maximum as well. Further, it has also been found [6] that when the focal spot is moved towards the ground electrode the time to the large pulse is less than if going the same distance towards the high voltage electrode. An explanation to this is that in the former case the first bubble/electrode connection is established by a fast, positive streamer. In the latter case the connection is made by slower, negative streamers. Time from large pulse to breakdown also depends on streamer polarity. If this time is short, it implies that the final connection is established by a positive streamer. Although it is clear from the current data when streamer connection takes place, this should not be mixed up with the time of streamer initiation. Even if a positive streamer is the first to connect due to its high speed of propagation, the negative streamers might be initiated

simultaneously with the positive ones. The questions of streamer initiation – how? and when? – are much more complicated.

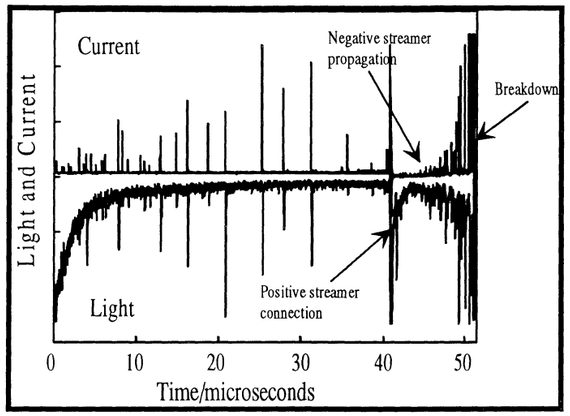

Figure 38. *Prebreakdown light and currents [6].*

Figure 39 shows what was hypothesized by Bäckman [6]. The numbers indicate in which order the streamer connect, while + and – denote streamer polarity. According to Bäckman, both streamers emanate from the cavity when the applied high voltage is positive. On the other hand, when the high voltage is negative only the second streamer starts propagating from the

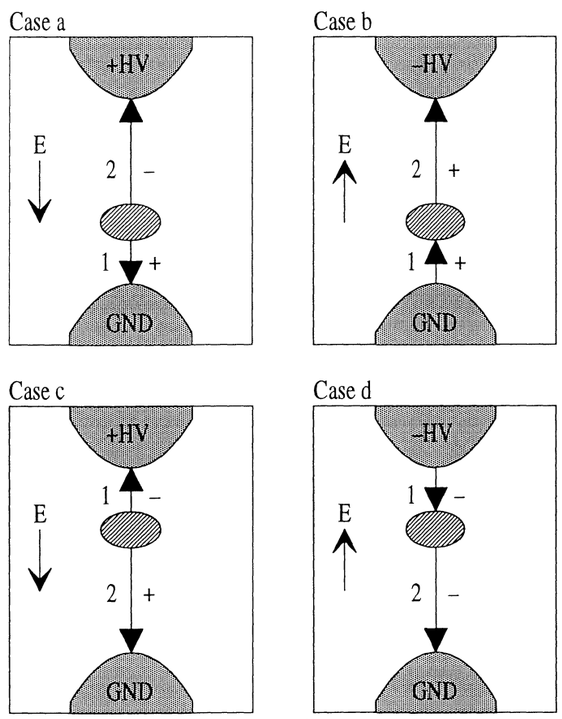

Figure 39. *Different streamer connections according to Bäckman [6]. Numbers indicate order of streamer connection, while + and – denote streamer polarity.*

cavity. The task was to verify these conclusions with pictures showing the different events. Laser pulses with an energy of 50 mJ were used. The interference filter did its duty, but no attenuation filter was necessary. Since the transformer oil was found to be contaminated again, it was replaced. Filtering was not sufficient this time.

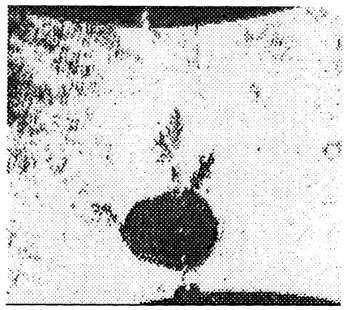

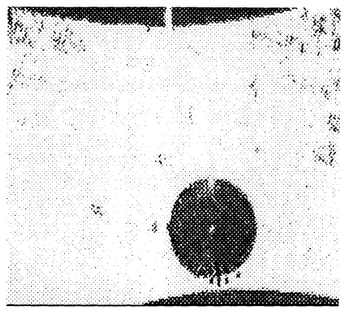

Figure 40 (left). *Positive and negative streamer propagation when subjected to positive high voltage. Bubble near ground electrode.*
Figure 41 (right). *Positive streamers near ground electrode.*

4.3.1 Case a

Starting with case a, +50 kV was applied to the 4.7 mm gap and the laser pulses were focused near the ground electrode. Figure 40 and 41 show examples of the situation. From Figure 40 it is clear that positive streamers connect the bubble to the ground electrode before any negative streamer has reached the upper, high voltage electrode. The picture was taken 70.32 µs after plasma initiation. The first positive streamer connection took place 66.32 µs after initiation, while breakdown occured 87.60 µs after initiation (if nothing else is stated, onwards all time data are given relatively to the time of plasma initiation). The extraordinary long time period between large pulse (positive streamer connection) and breakdown also points to the fact that the final connection is made by slow negative streamers. Figure 41 gives proof of existence of positive streamers prior to the existence of negative streamers. The picture was shot at 49.92 µs and a positive streamer connection was made 0.24 µs later. Breakdown followed at 77.20 µs. Conclusion: positive streamers emanating from the cavity are the first ones to connect. Negative streamers come later and bridge the remaining gap distance.

4.3.2 Case b

Polarity of the upper electrode was changed and –50 kV was applied to the gap. The focal spot was the same as in case a, i. e. near the ground electrode. In Figure 42 it is seen that, in this case, negative streamers take care of the first connection. In this particular picture, a negative streamer connected the bubble to the ground electrode at 51.52 µs. The picture was taken 8.00 µs later, 2.88 µs before breakdown. The outgrowths on top of the bubble are probably slow, bush-like positive streamers. Figure 43 shows a picture taken at exactly the same time as breakdown occurred, 59.44 µs after initiation. A negative streamer connection was made 9.12 µs earlier. Filamentous positive streamers can clearly be seen in the top part of the picture. Conclusion: negative streamers are the first ones to connect. They are followed by positive

streamers, which connect the bubble to the high voltage electrode. Both streamer types emanate from the vapour cavity.

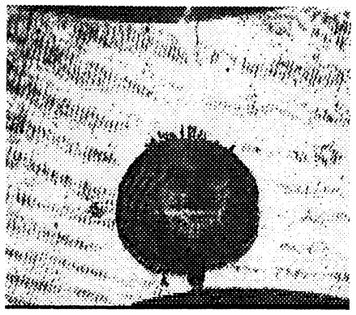

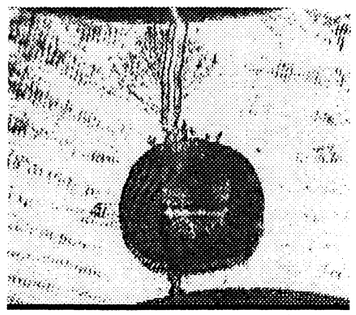

Figure 42 (left). *Negative streamers connected to the ground.*
Figure 43 (right). *Positive and negative streamer propagation when subjected to negative high voltage. Bubble near ground electrode.*

4.3.3 Case c

In this case the polarity again was positive. +50 kV was applied and the focal spot was moved to come close to the high voltage electrode (the distance between focal spot and electrode was approximately the same as in case a and case c). The picture shown in Figure 44 was taken at 72.80 µs. Simultaneously a positive streamer was connected to the ground. Breakdown was a fact 0.96 µs later. The positive streamer delta is evident near the ground electrode, but no negative streamers can be seen in the picture. Figure 45 shows a breakdown in action. Negative as well as positive connections can be seen. Note also the shock waves. This picture was shot 4.32 µs after breakdown, which happened at 77.60 µs. First streamer connection was made at 76.80 µs. Conclusion: succeeding positive streamers connecting to ground, negative streamers connect to the high voltage electrode.

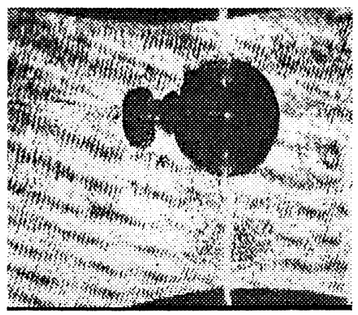

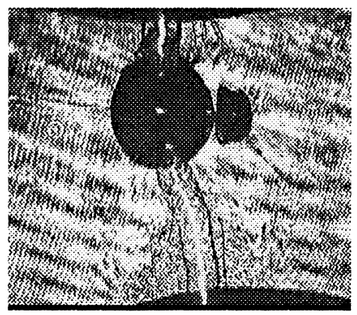

Figure 44 (left). *Positive streamers subjected to positive high voltage reaching for the ground.*
Figure 45 (right). *Breakdown in a positive high voltage gap. Bubble near high voltage electrode.*

4.3.4 Case d

Finally, the situation was ruled by –50 kV and a focal spot position near the high voltage electrode. Figure 46 shows positive streamers reaching for the high voltage electrode. The picture was taken at 56.88 µs, 1.68 µs before first streamer connection. Breakdown occurred much later at a time of 81.52 µs. The positive streamers caught here do not have their usual filamentary look, and seem much slower. It is also possible that the positive streamer that really made the connection is not visible in this picture. Anyway, negative streamers have not yet appeared. They can be seen in Figure 47, where they are propagating towards the ground electrode. The positive connection was made at 58.64 µs, 14 µs before the picture was taken. Breakdown took place 1.60 µs after the shot. Conclusion: first connection is made by a positive streamer. Final connection is made by a negative streamer. Both streamer types emanate from the vapour cavity.

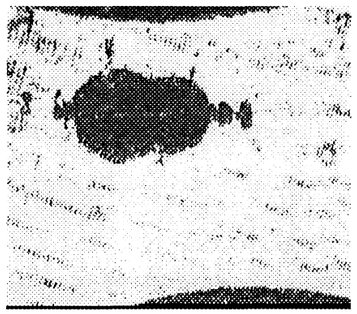

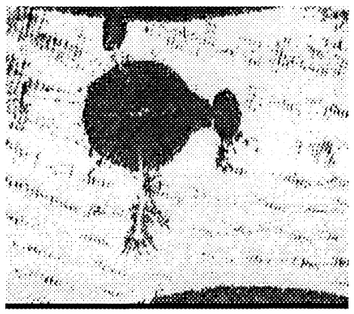

Figure 46 (left). *Positive streamers subjected to negative high voltage reaching for the high voltage electrode.*
Figure 47 (right). *Positive and negative streamer propagation when subjected to negative high voltage. Bubble near high voltage electrode.*

4.4 CONCLUSION

This chapter has offered several good pictures of streamers, showing that this phenomenon can be photographed rather easily. In addition, the propagation speed of negative streamers was estimated to be in the range of 200 m/s.

Figure 48 summarizes what has been found out about streamer connections in Section 4.3. If one compares with Bäckman's results (cf. Figure 39) there are a few differences. For example, even if the high voltage is negative both streamers seem to emanate from the cavity. No streamer comes from the electrodes. This difference also means that the polarity of some of the streamers is changed. Concerning case c, the streamer starting order is reversed. Recalling the initiation procedure of streamers, it is quite clear that negative streamers have to originate from the cavity, but why do positive streamers also behave like this?

It is evident from Figure 48 that the truth about streamer connections is not easy to figure out. A theory stating that the first streamer always connects to the nearest electrode does not agree

with reality (cf. case c), nor does a theory which states that the first connecting streamer is always positive (cf. case b).

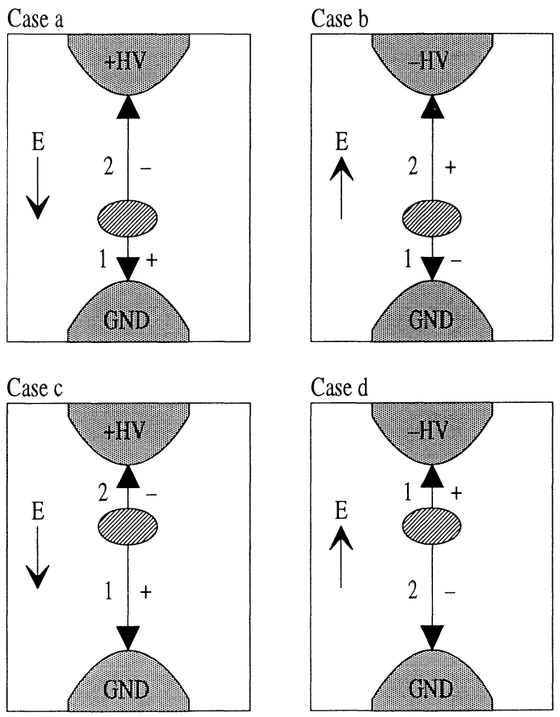

Figure 48. *Different streamer connections according to what was found in Section 4.3. Numbers indicate order of streamer connection, while + and – denote streamer polarity.*

Comparing case a with case d reveals a connection symmetry. Positive streamers connect first in both cases, but according to prebreakdown current data, the time between large pulse and breakdown (i. e. time from positive streamer connection to negative streamer connection) is almost twice as long in case a (~30 μs) as in case d (~15-20 μs). Following this fact, it seems like negative streamers in a negative electric field are faster than negative streamers in a positive electric field. In the same manner, comparing case b with case c, positive streamers in a negative electric field seem slow (time between large pulse and breakdown is ~10 μs in case b and ~1-2 μs in case c).

4.5 Prebreakdown Images on Photographic Film

This final section describes how the video camera was replaced by an ordinary Nikon system camera loaded with black and white photographic film with a sensitivity of 25 ASA. The objective was merely curiosity and a desire to investigate what such a method had to offer, particularly regarding picture resolution. Naturally, the computer was not at all involved during this kind of imaging. The camera used its self-timer and the exposure time was set to one second. An interference filter made sure that the film was only submitted to green light. The

sound from the camera shutter revealed when it was time to initiate breakdown, which was done for different values of the aperture stop of the camera as well as for different pulse energies of the green laser light. It was hard to know how much light was to expose the film to make a good result.

Figure 49 shows an enlargement of one of the pictures taken. The green laser light was unfortunately too weak to make the picture a real shadow-graph, but the bubble is clear as are the breakdown arc and the negative streamers. The laser initiation energy was 36 mJ and the applied voltage was +55 kV. As before, gap length was 4.7 mm. The picture was taken 75.28 µs after initiation. First streamer connection occurred 11.36 µs later and breakdown occurred after another 7.20 µs.

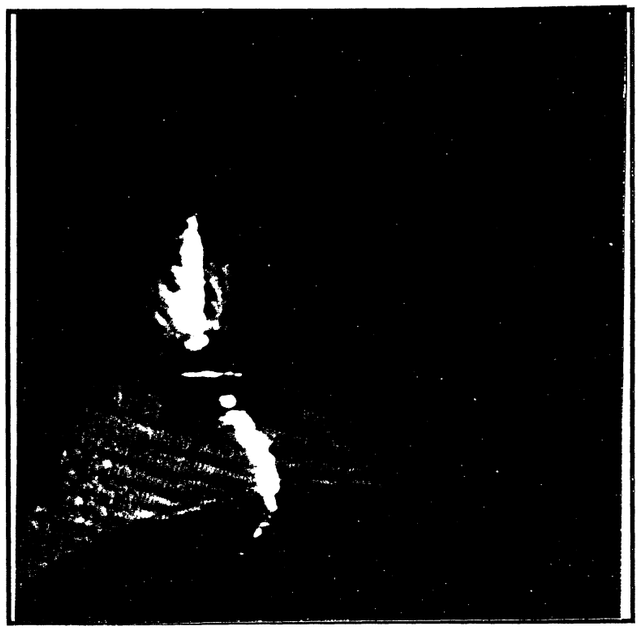

Figure 49. *Enlarged prebreakdown photographic picture.*

5. Discussion

5.1 Conclusion and Summary

First of all has this work shown the capability of the laser shadow imaging system, which proved to be a fine tool in the search for images of prebreakdown events. Thanks to the laser time resolution the system is able to image as fast courses as the propagation of a positive streamer. Therefore, all stages of the breakdown process have been imaged in this work, including bubble expansion and collapse, propagation of positive and negative streamers, and of course also the breakdown arc itself. The breakdown model derived by Bäckman [6] has been essentially verified, although a few corrections have been suggested concerning bubble growth and streamer connections.

It has been shown experimentally that bubble growth agrees well with the Rayleigh model of cavitation. This means that bubble radius in the early phase of expansion is proportional to the time of expansion raised to the power of 2/5. Most likely a linear relation exists between maximum bubble radius and initiation energy raised to the power of 3, although it was found that only about one percent of the total input laser energy is transferred to the bubble. The Rayleigh model of cavitation also states that bubble time of expansion is proportional to maximum bubble radius, which has been verified.

The vapour cavity is most certainly highly conducting. In spite of this, measurements have shown that it neither elongates nor grows due to the presence of a strong electric field. One possible reason for this is that time is too short in the sense that breakdown will occur long before the electrostatic forces will have time to act considerably. Thus the cavity expansion is totally driven by the vapour pressure.

Eventually, electrohydrodynamic instabilities of the cavity surface will cause negative streamers to be initiated. Positive streamers are thought to be initiated by means of the electric field. The electrohydrodynamic instabilities initially seem to be of microscopic size. It is a question of definition to tell when an instability is old enough to be called a negative streamer. Streamers will start propagating towards the nearest electrode that they "can see" (if the bubble is assumed to be opaque in this sense). It has been found that streamers, positive as well as negative, always emanate from the cavity, no matter the high voltage polarity and the electrode distance. They never start propagating from an electrode towards the cavity. The propagation speed of negative streamers has been estimated to be around 200 m/s, which is in agreement with results from other experiments. Experimental data indicate that negative streamers propagate faster in a negative electric field than in a positive. Similarly, positive streamers seem to propagate faster when the applied high voltage is positive. Regarding streamer connections in the case of positive or negative high voltage, as well as the case of different focal spot positions (bubble positions), the result can be found in Section 4.4, Figure 48.

5.2 Future Work

The most interesting remaining question is: what is the cause of streamer initiation? We have seen that it is not bubble elongation. Is there a critical electric field intensity at which initiation takes place? The bubble expansion leads to an increase in the mean electric field intensity, so it should be worthwhile to examine bubble size at exactly the time for streamer initiation, although this is not an easy task for the reasons of picture timing (cf. Section 3.4.3).

By using magnifying lenses and a non-interlaced camera, the picture resolution can be enhanced leading to sharper observations of positive streamers. Such observations can be helpful in determining the propagation speed of positive streamers.

Believe in future possibilities. Remember the words of Paul Simon [19]:
"These are the days of lasers in the jungle, lasers in the jungle somewhere."

6. Acknowledgements

I would like to thank the following persons for help and assistance while carrying out this work: my supervisor Anders Sunesson, my examiner Stefan Kröll, Åke Bergquist and Bertil Hermansson at the electronic workshop, Göran Werner at the mechanics workshop, Peter Bårmann, and Anders Persson.

7. References

1. D. Stålhandske, "Evaluation of a Method to Image a Laser-initiated Propagating Streamer," *Lund Reports on Atomic Physics*, 1996, LRAP- 171
2. A. Sunesson, P. Bårmann, S. Kröll, L. Walfridsson, "Laser Triggering of Electric Breakdown in Liquids," *IEEE Trans. El. Ins.*, 1994, Vol. 1, pp. 680-691
3. P. K. Watson, W. G. Chadband, W. Y. Mak, "Bubble Growth Following a Localised Electrical Discharge and its Relationship to the Breakdown of Triggered Spark Gaps in Liquids," *IEEE Trans. El. Ins.*, 1985, Vol. EI-20, pp. 275-280
4. L. Walfridsson, "A Triggered Spark Gap with Adjustable Energy," ABB Corporate Research, 1991, SERES/KJV/TR-91/094
5. P. Bårmann, "Spectroscopic Investigation of Streamers in a Dielectric Liquid," *Lund Reports on Atomic Physics*, 1996, LRAP-191, p. 8
6. J. Bäckman, "Light and Current Measurements from Prebreakdown Events in Laser-triggered Electrical Breakdown in Transformer Oil," *Lund Reports on Atomic Physics*, 1994, LRAP-150, pp. 61-77
7. E. Hecht, A. Zajac, *Optics*, Second Edition, Addison-Wesley, Reading, Massachusetts, 1987, pp. 316-319
8. A. Siegman, *Lasers*, University Science Books, Mill Valley, California, 1986, p. 676
9. R. B. Chapman, M. S. Plesset, "The Collapse of a Nearly Spherical Cavity in a Liquid," *Trans. ASME*, 1972, Vol. 94D, p. 142
10. R. Kattan, A. Denat, N. Bonifaci, "Formation of Vapor Bubbles in Non-polar Liquids Initiated by Current Pulses," *IEEE Trans. El. Ins.*, 1991, Vol. 26, pp. 659, 661
11. K. L. Stricklett, C. Fenimore, E. F. Kelley, H. Yamashita, M. O. Pace, T. V. Blalock, A. L. Wintenberg, I. Alexeff, "Observation of Partial Discharge in Hexane under High Magnification," *IEEE Trans. El. Ins.*, 1991, Vol. 26, p. 696
12. P. K. Watson, W. G. Chadband, M. Sadeghzadeh-Araghi, "The Role of Electrostatic and Hydrodynamic Forces in the Negative-point Breakdown of Liquid Dielectrics," *IEEE Trans. El. Ins.*, 1991, Vol. 26, pp. 545-554
13. M. Sadeghzadeh-Araghi, M. I. Qureshi, W. G. Chadband, P. K. Watson, "Measurement of the Growth of Cavities and of EHD Instabilities during the Negative-point Breakdown of Silicone Fluids," *IEEE Trans. El. Ins.*, 1991, Vol. 26, pp. 663-672
14. H. Borsi, E. Gockenbach, U. Schröder, G. Schiller, "Contribution to the Clarification of Partial Discharge Behaviour in Insulating Liquids Using the Schlieren Technique," *ETEP*, 1991, Vol. 1, pp. 271-279
15. M. I. Qureshi, W. G. Chadband, "On the Relation Between Current Pulses and Discharges," *IEEE Trans. El. Ins.*, 1988, Vol. 23, pp. 715-722
16. C. G. Garton, Z. Krasucki, "Bubbles in Insulating Liquids: Stability in an Electric Field," *Proc. Roy. Soc. A*, 1964, Vol. 280, pp. 211-226
17. A. Beroual, "Behavior of Charged and Uncharged Bubbles in Dielectric Liquids Subjected to Electric Stress," *J. Appl. Phys.*, 1992, Vol. 71, pp. 1142-1145
18. G. S. Kath, J. F. Hoburg, "Interfacial EHD Instability in Normal Electronic Fields," *Phys. Fluids*, 1977, Vol. 20, pp. 912-916

19. P. Simon, The Boy in the Bubble, Graceland, 1986